

THESIS

A MASS BALANCE APPROACH TO RESOLVING
THE STABILITY OF LNAPL BODIES

Submitted by

Nicholas T. Mahler

Department of Civil and Environmental Engineering

In partial fulfillment of the requirements

For the Degree of Master of Science

Colorado State University

Fort Collins, Colorado

Summer 2010

COLORADO STATE UNIVERSITY

JUNE 16, 2010

WE HEREBY RECOMMEND THAT THE THESIS PREPARED UNDER OUR SUPERVISION BY NICHOLAS T. MAHLER ENTITLED A MASS BALANCE APPROACH TO RESOLVING THE STABILITY OF LNAPL BODIES BE ACCEPTED AS FULFILLING IN PART REQUIREMENTS FOR THE DEGREE OF MASTER OF SCIENCE.

Committee on Graduate Work

Domenico A. Bau

David B. McWhorter

Advisor: Thomas C. Sale

Department Head: Luis Garcia

ABSTRACT OF THESIS
A MASS BALANCE APPROACH TO RESOLVING
THE STABILITY OF LNAPL BODIES

Light non-aqueous phase liquids (LNAPLs) are commonly present in soils and groundwater beneath petroleum facilities. When sufficient amounts of LNAPL have been released continuous bodies of LNAPL form. These bodies can have detrimental impacts to soil gas and groundwater. Furthermore, with time they can expand or translate laterally. Measurements of LNAPL flux within continuous bodies typically indicate that LNAPL is moving, albeit slowly. Commonly, these fluxes have been used to infer (by continuity) that the bodies as a whole are expanding and/or translating laterally. In conflict with this, dissolved plumes downgradient of LNAPL bodies are widely thought to be stable or shrinking due to natural attenuation. The hypothesis of this research is that natural losses of LNAPL in contiguous bodies can play an important role in limiting expansion and/or lateral translation of LNAPL bodies. Much like dissolved phase plumes, LNAPL bodies can be stable when internal fluxes are balanced by natural losses.

As a first step, 50 measurements of LNAPL fluxes through wells from seven field sites are reviewed. All the values were acquired using tracer dilution techniques. The mean and median of the LNAPL flux measurements are 0.15

and 0.064 m/year, respectively. The measured LNAPL fluxes are three to five orders of magnitude less than typical groundwater fluxes. The primary significance of the small magnitude of the LNAPL fluxes relative to groundwater fluxes is that LNAPL discharge to the downgradient body could easily be equal to or less than the natural downgradient LNAPL losses that occur through dissolution into groundwater or evaporation into soil gas. In general no clear correlations are seen between measured LNAPL fluxes and LNAPL thicknesses in wells, lengths to downgradient edges of LNAPL, or the specific gravities (density of LNAPL/ density of water) of the LNAPL.

Secondly, a proof-of-concept sand tank experiment is presented. The objective was to resolve if natural LNAPL losses can limit expansion of an LNAPL body given a constant source. An open top glass and stainless steel tank (1 m by 0.5 m by 0.025 m) was filled with uniform coarse sand and water. Water was pumped through the tank producing a water seepage velocity of 0.25 m/day. Methyl tert-butyl ether (MTBE) was added to the tank at constant rates that were step-wise increased five times through a 120 day experiment. In all cases the MTBE body initially expanded followed by subsequent stabilization at a finite length. The key observation was that steady LNAPL pool lengths were achieved with a constant inflow of LNAPL into the system.

Lastly, analytical models are developed. The models describe the size of LNAPL bodies and spatial variations in LNAPL fluxes as a function of influent loading, rates of natural losses, and time. Three idealized geometries of LNAPL bodies are considered. These include one dimensional, circular, and oblong.

Results indicate LNAPL fluxes decline progressing from the interior to the edges of an LNAPL body. Per the laboratory studies, the solutions show that LNAPL bodies with a constant source reach finite dimensions at large times. Building on this research it seems that a pragmatic goal for management of contiguous LNAPL bodies is attaining a condition where the LNAPL bodies as a whole are stable or shrinking.

Nicholas T. Mahler
Department of Civil and Environmental Engineering
Colorado State University
Fort Collins, CO 80523
Summer 2010

This thesis is dedicated to David M. Gilbert for all his support and guidance.

He will never be forgotten.

Acknowledgements

A number of individuals extended their support, aid, and expertise in the development of this thesis.

- First and foremost I would like to extend my utmost gratitude to Dr. Tom Sale, for serving as the advisor for this work and his patience and guidance in the development of this thesis.
- Dr. Domenico Bau and Dr. David McWhorter for serving on the advisory committee.
- Dr. Julio Zimbron and Mitchell Olson for their technical support.
- Jillian Hume from CH2M Hill for her patience and aid with me during field measurements of LNAPL fluxes.
- Arthur Corey for his scholarship and input.
- My family and friends for all the support and encouragement they gave.

Funding for this work was provided by:

- Chevron
- American Petroleum Institute
- Suncor Energy
- Exxon Mobil

Table of Contents

1	INTRODUCTION.....	1
2	SINGLE WELL TRACER DILUTION TESTS TO EVALUATE FIELD LNAPL FLUXES	5
2.1	ABSTRACT.....	5
2.2	INTRODUCTION	6
2.3	METHODS	8
2.3.1	<i>Field Sites</i>	8
2.3.2	<i>Field Methods</i>	11
2.3.3	<i>Data Analysis</i>	16
2.4	RESULTS AND DISCUSSION.....	19
2.5	CONCLUSIONS.....	25
2.6	ACKNOWLEDGEMENTS	27
3	A MASS BALANCE APPROACH TO RESOLVING LNAPL STABILITY	28
3.1	ABSTRACT.....	28
3.2	INTRODUCTION	29
3.3	LABORATORY STUDY	31
3.3.1	<i>Materials and Methods</i>	31
3.3.2	<i>Results and Discussion</i>	34
3.4	THEORY.....	39
3.4.1	<i>Extent</i>	40
3.4.2	<i>Fluxes</i>	44
3.4.3	<i>Comparison with Laboratory Data</i>	47
3.5	MODEL APPLICATION	49
3.5.1	<i>Extent vs. Time</i>	49
3.5.2	<i>Flux Throughout the LNAPL Body</i>	53
3.6	CONCLUSIONS.....	56
3.7	ACKNOWLEDGEMENTS	58
4	CONCLUSIONS.....	59
5	FUTURE WORK	63
5.1	TRACER DILUTION FLUX MEASUREMENTS.....	63
5.2	ANALYTICAL MODELS	65
6	REFERENCES.....	67
	APPENDIX A LNAPL TRACER DILUTION TESTS.....	A.1
	APPENDIX A.1 EXAMPLE C_T/C_0 DATA	A.1

APPENDIX B	LABORATORY EXPERIMENT	B.1
APPENDIX B.1	PROOF-OF CONCEPT STUDY REDUCED DATA.....	B.1
APPENDIX C	THEORY	C.1
APPENDIX C.1	ONE-DIMENSIONAL EXTENT V. TIME DERIVATION.....	C.1
APPENDIX C.2	TWO-DIMENSIONAL EXTENT V. TIME DERIVATION	C.4
APPENDIX C.3	ONE-DIMENSIONAL FLUX DERIVATION.....	C.8
APPENDIX C.4	TWO-DIMENSIONAL FLUX DERIVATION.....	C.10

List of Figures

Figure 2.1 - Site maps depicting with LNAPL extent, surface water bodies, and groundwater flow direction, and tracer dilution test wells.....	10
Figure 2.2 - Representative intensity versus wavelength signal of Stay-Brite BSL-715.	12
Figure 2.3 - Flow chart of the installation and initiation of a petroleum hydrocarbon tracer study.....	13
Figure 2.4 - a.) Isolation of known tracer concentrations in pipes and b.) periodic mixing during a sampling event (Smith, 2008).....	14
Figure 2.5 - Procedure for intermittent LNAPL tracer dilution tests.....	15
Figure 2.6 - Representative normalized intensity versus time data set with a linear regression.	17
Figure 2.7 - Histogram of the measured fluxes at the seven sites.	21
Figure 2.8 - Comparison of LNAPL thickness in wells to LNAPL fluxes for sites A-F.....	22
Figure 2.9 - Specific gravity of LNAPL at sites A-F plotted against LNAPL flux..	23
Figure 2.10 - A presentation of the relationship between the length to the downgradient pool edge and LNAPL flux.	24
Figure 2.11 - Histogram showing the distribution of calculated loss rates to the LNAPL bodies assuming the bodies are stable.	25
Figure 3.1 - Experimental setup for evaluating the expansion on an LNAPL body with a constant source.....	33
Figure 3.2 - Expansion of the continuous MTBE body exposed to losses due to dissolution and evaporation.....	35
Figure 3.3 - Best fit logarithmic trend lines for the MTBE length versus time.	36
Figure 3.4 - Rate of change of the length of the MTBE body versus time.	37
Figure 3.5 - Mass balance performed to determine the relative influence of dissolution and evaporation on the stability of the MTBE body.	38
Figure 3.6 - Conceptual basis for mass balance. The a.) one-dimensional, b.) circular, and c.) oblong geometries are shown, as well as the d.) cross-sectional view associated with all three geometries.	40
Figure 3.7 - Visual representation of the REVs for the a.) one-dimensional and b.) radially symmetric two-dimensional cases. The one-dimensional case is	

shown in a.), where Δx is the length, w is the width. The circular and oblong REV is shown in b.), where r is the inner radius of the REV, R is the outer radius of the REV, and θ is the angle of the REV.....	45
Figure 3.8 - Comparison between the observed steady-state LNAPL lengths and predicted LNAPL lengths.....	48
Figure 3.9 - The top panels (a, b, and c) show expansion of the leading edge of the two dimensional oblong body versus time. The bottom panels (d, e, and f) show the change in length per time versus time of the leading edge. Input parameters: $b = 0.3 \text{ m}$, $r_s = 0.3 \text{ m}$, $S = 0.3$, $S_r = 0.001$, $\phi = 0.001$	50
Figure 3.10 - Comparison of the effects of inflow rate and loss rates on the extent over time of an oblong LNAPL body. Input parameters: $b = 0.3 \text{ m}$, $r_s = 0.3 \text{ m}$, $S = 0.3$, $S_r = 0.001$, $\phi = 0.001$. The contours are given in years. The contour time increments are: 40 yrs for panels a, b, and c, 20 yrs for panels d, e, f, and 10 yrs for panels g, h, i.....	52
Figure 3.11 - Predicted flux profile of the oblong solution on the center line parallel to groundwater flow.....	54
Figure 3.12 - Predicted flux contours over the extent of an oblong LNAPL body, by varying the release rate and loss rate. Input parameters: $b = 0.3 \text{ m}$, $r_s = 0.3 \text{ m}$, $S = 0.3$, $S_r = 0.001$, $\phi = 0.001$	55
Figure C.1 - One dimensional extent.....	C.1
Figure C.2 - Conceptual extent figures for the circular and oblong cases.	C.4
Figure C.3 - REV for one-dimensional flow.	C.8
Figure C.4 - REV for two-dimensional flow.....	C.10

List of Tables

Table 2.1 - Summary of site data and measured LNAPL flux values (note: < represents less than and N/A represents not applicable).	20
Table 3.1 - Porous media parameters.	32
Table 3.2 - Steady-state injection length at each injection location and rate.	35
Table 3.3 - Loss rates due to evaporation and dissolution.	38
Table 3.4 - Boiling point and relative persistence data for common LNAPLs (Scholz et al., 1999).....	39
Table 3.5 - Time, in years for a contiguous LNAPL body to stabilize.....	51
Table B.1 - Reduced proof-of-concept data.....	B.1

1 Introduction

Over the past century on the order of 10^7 cubic meters of petroleum liquids have been produced, refined, and utilized (Energy Information Administration, 2010). This has added great convenience to modern life. A result of our use of petroleum liquids has been inadvertent releases to the soil and groundwater. Petroleum liquids in the subsurface are referred to as light non-aqueous phase liquids (LNAPLs). Concern has arisen as to the potential for LNAPLs to impact groundwater and soil gas, as well as the possible expansion or lateral translation of bodies of continuous LNAPL.

Due to potential adverse impacts from LNAPL, methods have been developed to remediate subsurface LNAPL bodies. Unfortunately, complete removal of LNAPL is difficult (Sale, 2003). Starting in the 1990s the primary goal for LNAPL releases was recovery to the extent practicable. This goal has often been defined in terms of minimum thicknesses in monitoring wells (e.g. ITRC, 2009). The relationships between thicknesses in wells, amount of LNAPL in the formation, and the stability of LNAPL is complex (e.g. Farr et al., 1990 and Lenhard and Parker, 1990). This has caused the performance metric of LNAPL thicknesses in wells to be burdened with difficulties. The challenges with using thicknesses in wells as a performance metric has caused the American Petroleum Institute and researchers to explore alternative methods for

determining LNAPL recovery to the extent practicable. Considerable attention has been given to LNAPL flux as an alternative metric for evaluating LNAPL remedies. LNAPL flux is defined as a volume of fluid moving through a unit cross-section (perpendicular to flow) per unit time. The potential to use flux as a performance metric has led to development of tools to measure LNAPL flux. The majority of these tools rely on measurements of formation conductivity and head gradients through LNAPL bodies (Charbeneau, 1999 and Sale, 2003). Using Darcy's equation the product of these values provides an estimate of LNAPL flux. An alternative approach to estimate LNAPL flux is the use of tracers and single well tracer dilution techniques (Taylor, 2004; Sale et al., 2007a; Sale et al., 2007b; Sale et al., 2008; Smith, 2008; and Smith et al., 2010). Commonly LNAPL fluxes are found to be orders of magnitude less than typical groundwater fluxes (Sale, 2003). The second section of this thesis reviews the use of tracers to measure 50 LNAPL fluxes at seven field sites.

A common practice has been to assume (by continuity) that a point LNAPL flux measurement is reflective of the flux throughout a contiguous body. This is analogous to interpretation of groundwater fluxes, in which a flux measurement is extended through a uniform groundwater flow field. Extrapolating measured LNAPL fluxes throughout the body leads to the expectation that the LNAPL body should be expanding and/or translating. Contrary to this interpretation dissolved phase plumes downgradient of LNAPL bodies are commonly stable. Natural attenuation of the plumes is believed to control their stability (e.g. Weidemeir et al., 1999). Monitored natural attenuation

has become a widely accepted remedial action for the dissolved phase plumes (National Research Council Committee on Intrinsic Remediation, 2000), yet many regulatory agencies still require the LNAPL bodies to be depleted (ITRC, 2009). However, even with losses, if the continuous LNAPL bodies feeding these plumes are migrating, the plumes themselves would also migrate. It appears that the internally measured LNAPL fluxes and the observation of stable dissolved phase plumes are potentially in conflict.

The principle hypothesis of this thesis is that natural losses of LNAPL due to dissolution and evaporation play an important role in controlling expansion and/or lateral translation of LNAPL bodies. Similar to dissolved phase contaminant plumes, LNAPL bodies become stable when inflows (measured as upgradient LNAPL fluxes) are balanced by losses in downgradient bodies. This leads to the idea that a stable or shrinking LNAPL body is a promising remedial objective for subsurface LNAPL bodies.

This thesis explores the possible influence of losses on the stability of continuous LNAPL bodies. Two chapters are presented. Both are written in a journal article format and will be submitted to the journal of Ground Water[®] for publication. The first chapter presents LNAPL flux measurements from seven field sites using tracer dilution techniques. This chapter illustrates the existence of small LNAPL fluxes at field sites and their dependence on LNAPL thicknesses in wells, specific gravities, and lengths to the downgradient edge of the LNAPL body. The second chapter presents a proof-of-concept laboratory experiment that evaluates the effects of losses on the stability of an LNAPL body followed by

development and application of analytical models that describe governing processes under idealized conditions. The final sections of this thesis provide a summation of the information presented and recommendations for further work.

2 Single Well Tracer Dilution Tests to Evaluate Field LNAPL Fluxes

2.1 Abstract

Petroleum liquids, referred to as light non-aqueous phase liquids (LNAPLs), are commonly found beneath petroleum facilities. Concern with LNAPLs can include further migration into clean soils, movement off site, and discharges to surface water. LNAPL thickness in wells has commonly been the metric used for evaluating LNAPL stability. However, the relationship between LNAPL thickness in wells and the stability of LNAPL bodies is complex. This complexity has led to the consideration of LNAPL flux as an alternative metric for LNAPL stability.

Single well tracer dilution techniques were used to measure LNAPL fluxes in 50 wells at seven field sites. A hydrophobic tracer was mixed into LNAPL in a well. Intensities of the tracer signal were measured over time using a spectrometer and fiber optic cable. Tracer concentrations are proportional to fluorescence intensities over the range of the measured values in question. LNAPL fluxes were found using changes in the tracer concentrations through time.

Measured LNAPL fluxes range from 0.006 to 2.6 m/yr with a mean and median of 0.15 and 0.064 m/yr, respectively. The measured LNAPL fluxes are

three to five orders of magnitude smaller than typical groundwater fluxes (e.g. 10 to 100 m/yr). Relationships between LNAPL fluxes and possible governing parameters were evaluated. In general LNAPL fluxes are independent of LNAPL thickness in a well, the specific gravity of the LNAPL, and the distance to the downgradient edge of the LNAPL body. Potential LNAPL loss rates were calculated based on the assumption of a stable LNAPL body and the lengths to the downgradient edge of the body. The mean (24.0 m³/ha/yr) and median (5.0 m³/ha/yr) of potential LNAPL loss rates were calculated to be above or within a range of field measured loss rates (1.25 to 12.5 m³/ha/yr).

2.2 Introduction

Petroleum liquids are commonly found beneath petroleum production, refining, distribution, and storage facilities. These liquids are referred to as light non-aqueous phase liquids (LNAPLs). A primary concern with LNAPLs is their subsurface stability. LNAPL stability issues can include impacts to clean soils, off site migration, and discharges to surface water. This paper presents LNAPL flux measurements obtained from 50 wells at seven petroleum facilities (field sites). The measurements were obtained using single well tracer dilution techniques.

Historically, thickness of LNAPL in wells has been a primary metric for evaluating the stability of continuous LNAPL bodies (e.g. ITRC, 2009). Unfortunately, the relationship between LNAPL thickness in wells and LNAPL stability is complex (e.g. Farr et al., 1990 and Lenhard and Parker, 1990). This

complexity has led to an alternative approach wherein LNAPL flux has been considered as a metric for evaluating LNAPL stability (Sale, 2003). LNAPL flux, as described herein is a volume of fluid moving through a unit cross-section (normal to flow) per unit time.

Methods for determining LNAPL fluxes include use of Darcy's equation and single well tracer dilution techniques. Darcy based approaches rely on the product of an LNAPL conductivity term and the gradient of head through an LNAPL body. LNAPL conductivity values can be estimated via collection and analysis of core samples (e.g. Sale, 2001), baildown tests (Huntley, 2000), and pumping tests (Sale, 2001). Gradients of LNAPL head are estimated using the water table gradient through an LNAPL body or the measured elevation of LNAPL-air interfaces in wells. As described by Smith (2008) assumptions associated with both approaches can lead to significant errors in estimating the gradient of LNAPL head.

Given the challenges with Darcy based approaches single well tracer dilution techniques (tracer dilution tests) have been developed to measure LNAPL flux (Taylor, 2004; Sale et al., 2007a; Sale et al., 2007b; Sale et al., 2008; Smith, 2008; and Smith et al., 2010). The use of tracers to determine LNAPL fluxes builds on borehole tracer dilution techniques presented in Freeze and Cherry (1979). The concentration of tracer through time is used to resolve LNAPL flux through a well. Methods developed by Taylor (2004) require continuous mixing and measurement of tracer concentration. Smith (2008) built off of the concepts brought forth by Taylor (2004) by developing methods

involving intermittent mixing and monitoring. Advantages of the methods presented in Smith (2008) include simplicity of equipment and the ability to concurrently conduct a large number of tracer dilution tests at a single field site.

The primary purpose of this paper is to present 50 LNAPL flux measurements obtained from wells at seven field sites. This provides a unique compilation of LNAPL flux measurements for a range of site conditions. A secondary purpose is to present field methods for conducting single well tracer dilution tests.

2.3 Methods

The following advances methods used to measure 50 LNAPL flux in wells at seven sites. First, the field sites are described. Secondly, field methods for conducting single well tracer dilution tests are presented. Field data was acquired through collaborative efforts between Colorado State University and those identified in the acknowledgements section of this paper.

2.3.1 Field Sites

A total of seven field sites are considered. Detailed information regarding the site locations have been removed in accordance with collaborators' requests. Maps showing LNAPL extent, surface water bodies, groundwater flow directions, and tracer dilution test wells at six of the sites are presented in Figure 2.1. The seventh site involves a single well in an extensive LNAPL body adjacent to a river. Six of the sites are located adjacent to water bodies that impact groundwater levels. One of the sites is tidally influenced. Five of the seven sites

are along rivers with seasonal variations that impact groundwater levels. All sites are underlain by sandy alluvium. Depths to water and LNAPL range from 3 to 8 m. LNAPL encountered at the seven sites range from light ends including gasoline and diesel to heavy ends including fuel oils and lubricants. Active releases at all sites have been addressed and the encountered LNAPLs have been present in the subsurface for decades. Additional information is presented in tabular form in the results section of this paper.

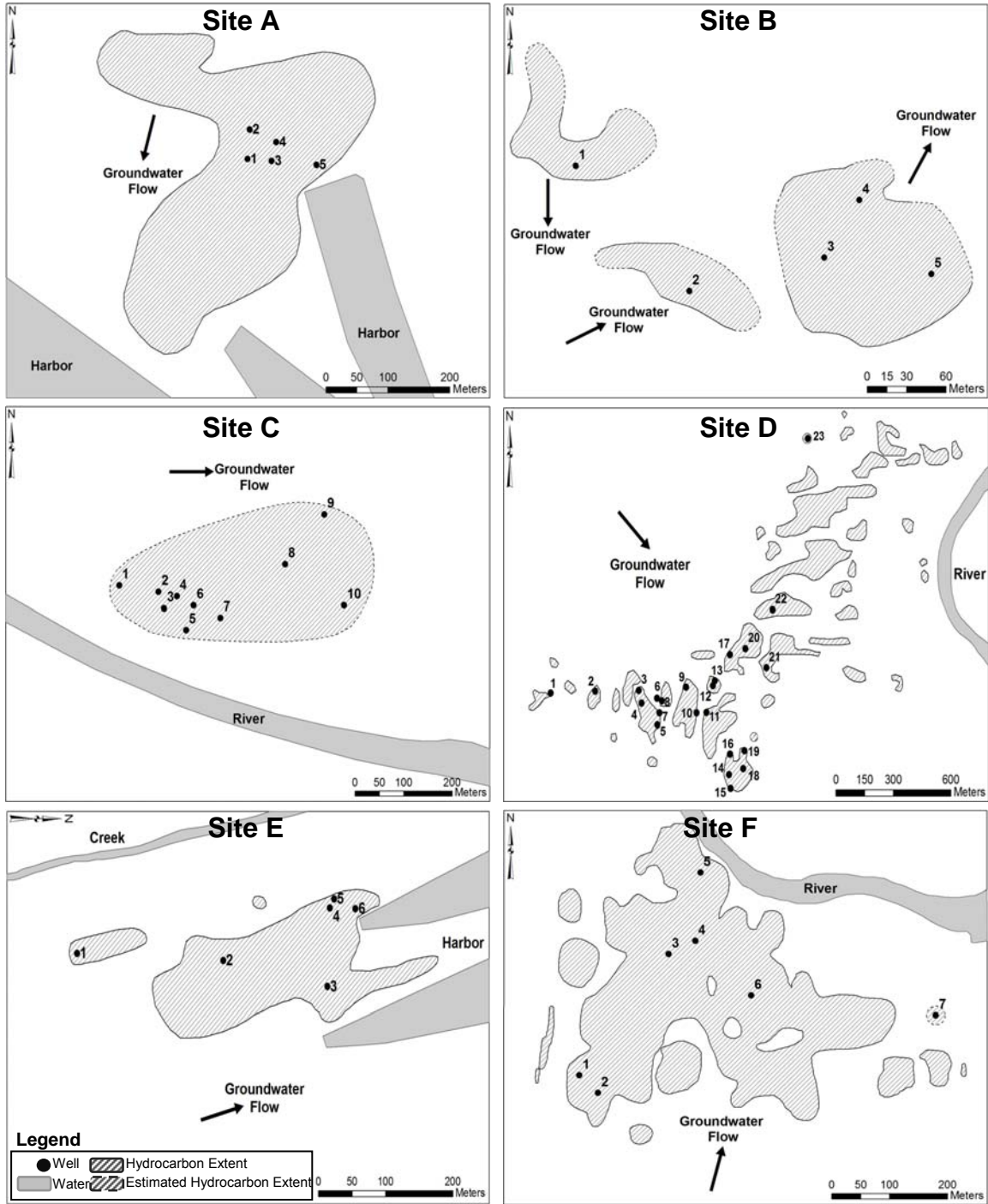


Figure 2.1 - Site maps depicting with LNAPL extent, surface water bodies, and groundwater flow direction, and tracer dilution test wells.

2.3.2 *Field Methods*

Following Smith (2008), procedures for conducting LNAPL tracer dilution test involve placing a tracer into LNAPL in a well and recording tracer concentrations as a function of time. Tracer concentrations are measured using a spectrometer, fiber optic cable, and in-well LNAPL standards with background and initial (i.e. 0 and 100%) tracer concentration. Mixing at six of the sites was conducted using intermittent mixing techniques (Smith, 2008). The seventh site relied on continuous mixing techniques developed by Taylor (2004). Given that this method has been replaced by Smith (2008) it is not included herein. The following text describes each of the steps in detail.

Selection of Test Wells – Initially, data from wells with LNAPL at each of the sites was acquired and reviewed. Water levels and LNAPL thicknesses were evaluated as a function of time. Furthermore well completions were reviewed to verify that the LNAPL was in the screened interval of the wells. Prior to initiating a tracer dilution test, samples of LNAPL were collected. LNAPL samples were analyzed for background fluorescence and calibration curves were developed to resolve the amount of tracer needed to achieve fluorescence peaks at 545 and 580 nm that were two to three times greater than the background. Methods for measuring fluorescence are presented in the following text.

The fluorescing tracer used was Stay-Brite BSL 715 (Bright Solutions Inc., Troy, Michigan). Stay-Brite BSL-715 is a hydrophobic dye used in the automotive industry to detect engine leaks. A representative graph of intensity versus wavelength for an LNAPL with background and tracer fluorescence is

presented in Figure 2.2. Through the course of the field tests three different Ocean Optics spectrometers were used (USB 2000, USB 4000, and Jazz; Dunedin, Florida). Each were equipped with a 470 nm ($1 \text{ nm} = 10^{-9} \text{ m}$) light source. Data was acquired from the spectrometer using both a laptop computer and Ocean Optics OOIBase32 or Spectra Suites software. In all cases an Ocean Optics six around one fiber optic cable with a reflectance probe was employed. The six outer fibers conveyed the 470 nm light source to the LNAPL in the well. The center fiber then carried the fluorescent signal back to the spectrometer. According to Taylor (2004) and Smith (2008) the intensity of fluorescence is linearly proportional to tracer concentration over the range of interest for the tracer dilution tests. With this, intensity was used as a direct indicator of fractional changes in tracer concentrations.

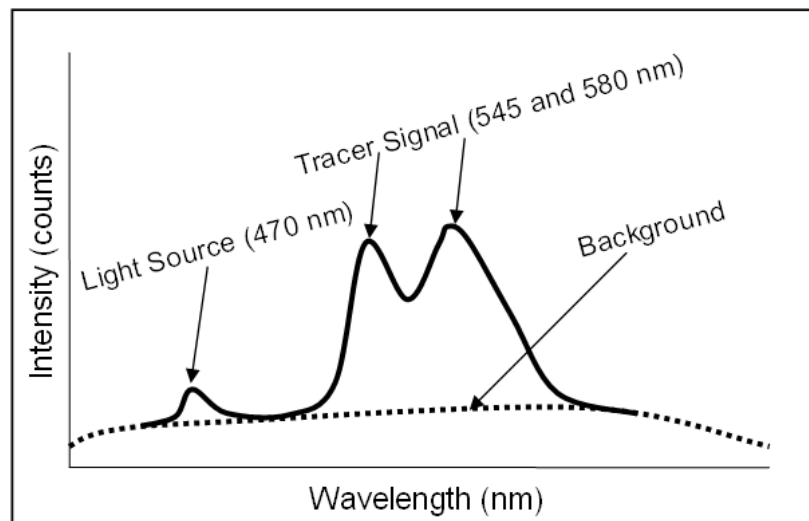


Figure 2.2 - Representative intensity versus wavelength signal of Stay-Brite BSL-715.

Setup – To initiate the single well tracer dilution test, a small diameter (e.g. 1.27 cm) PVC pipe was lowered into a well isolating LNAPL with no tracer. This standard (C_0) allowed for measurement of background fluorescence

throughout the test. Next, tracer was added, taking care to prevent tracer from contacting the well casing above the fluid levels in the well. Typical tracer concentrations were 1-10 parts per thousand. Once added the tracer was thoroughly mixed in the LNAPL using an air bubble line. Complete mixing of tracer was verified by slowly raising and lowering the probe through the LNAPL column while recording intensity at 545 and 580 nm. After achieving uniform tracer concentrations, a second standard pipe (C_{100}) was placed through the LNAPL to isolate LNAPL with initial tracer concentrations. The two in-well standards (C_o and C_{100}) were used to calibrate the spectrometer each time tracer concentrations were measured in the well. The above steps are outlined in Figure 2.3 and shown in panel a of Figure 2.4.

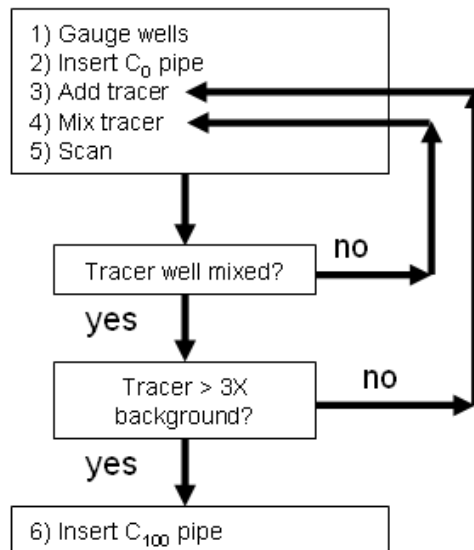


Figure 2.3 - Flow chart of the installation and initiation of a petroleum hydrocarbon tracer study.

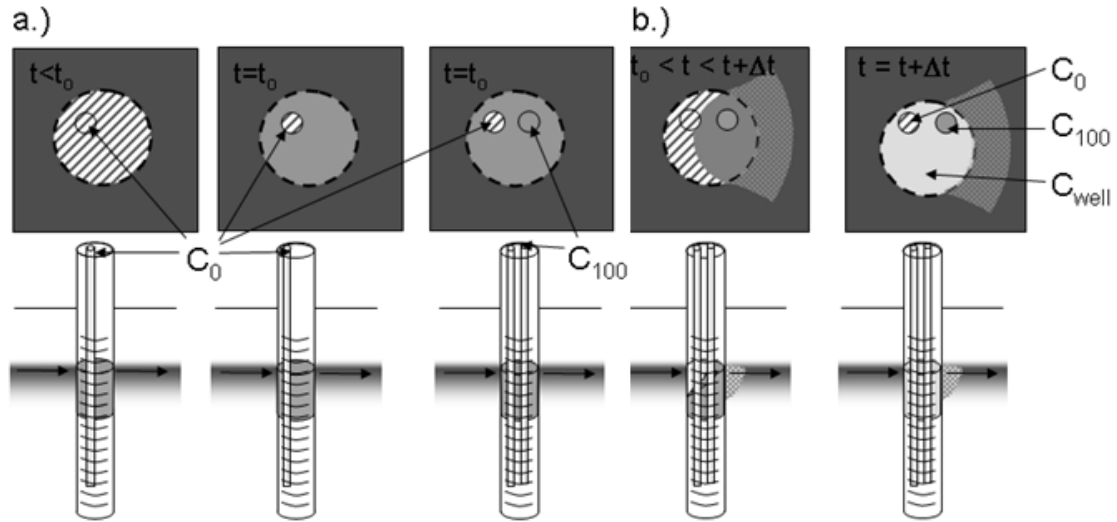


Figure 2.4 - a.) Isolation of known tracer concentrations in pipes and b.) periodic mixing during a sampling event (Smith, 2008).

Scanning Procedure – Scanning refers to measuring tracer concentrations of the well (C_{well}) and the in-well standards (C_0 and C_{100}). The first scanning event occurred after the initial addition of tracer to the well. Subsequent scanning was based on seeing greater than one percent and less than ten percent change in tracer concentrations. Between scanning events LNAPL moved from the formation into the well, displacing a portion of LNAPL with tracer from the well. Thus, the concentration of tracer in the well decreased with time. Panel b in Figure 2.4 illustrates the conditions in the well during scanning events.

The scanning procedure is outlined in Figure 2.5. The measurement of fluorescence intensity was performed by lowering the fiber optic cable into the well or in-well standards. Excitement of the tracer was measured in intensities and directly associated with the tracer concentration. The measured intensities were associated with the concentration of tracer. Subsequently, tracer

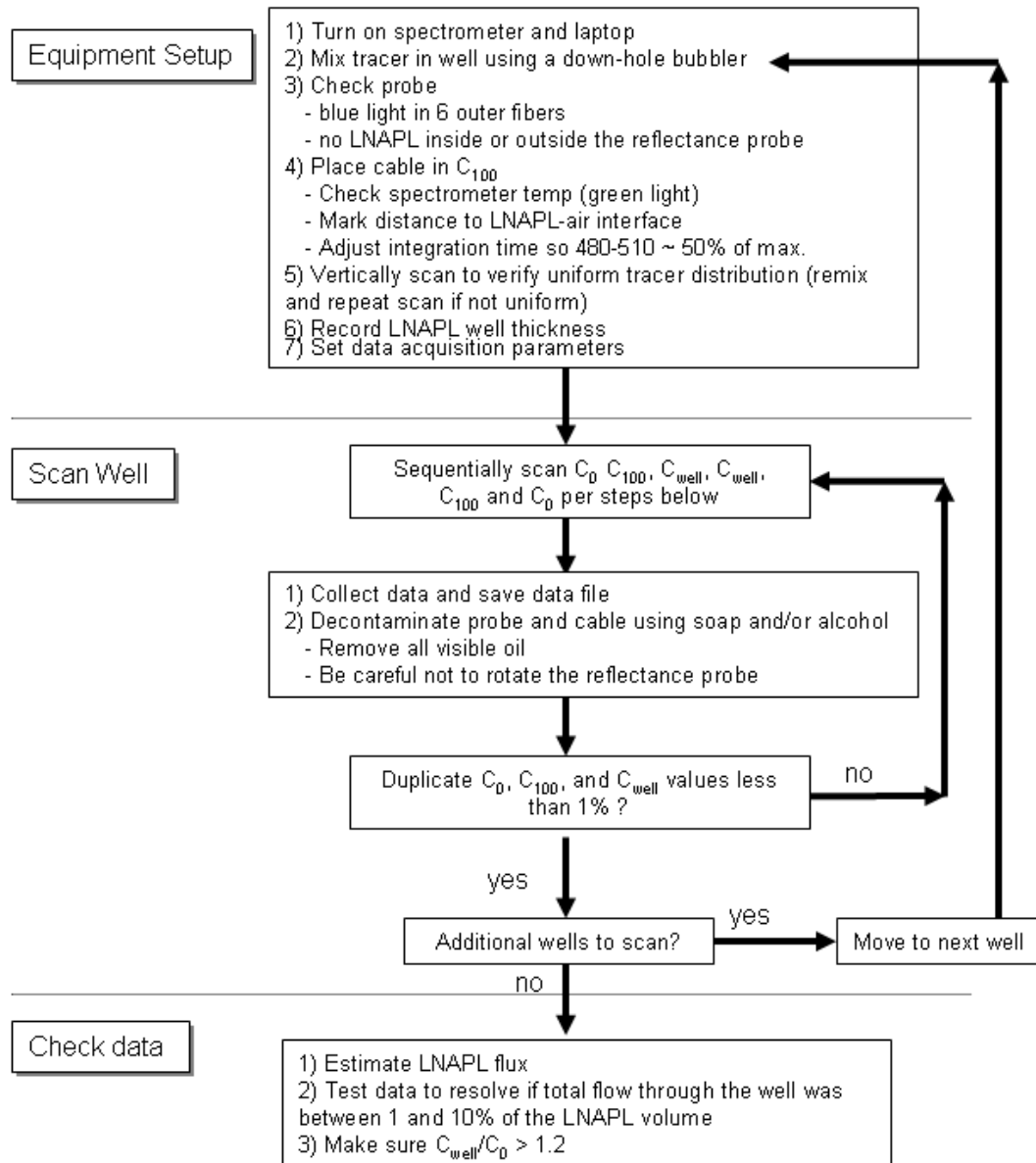


Figure 2.5 - Procedure for intermittent LNAPL tracer dilution tests.

concentrations (intensities) were measured in following sequence: C_0 , C_{100} , C_{well} , C_{well} , C_{100} , and C_0 . Duplicate measurements were made to verify uniform mixing in C_{well} and C_{100} and to verify the operation of the fiber optic cable and spectrometer. The goal for the percent difference between duplicate measurements was one percent or less. Between measurements of C_0 , C_{100} ,

and C_{well} the probe was cleaned using soap and/or alcohol to prevent carrying tracer between the standards and the wells.

Tracer data was validated by ensuring the tracer signal decreased within one to ten percent between measurements and remaining tracer was 20% greater than the background intensity. Following Smith (2008), less than ten percent tracer loss between measurements is desired when using intermittent mixing techniques.

2.3.3 Data Analysis

A linear regression was fit to the normalized concentration versus time data. The normalized concentration is defined as $((C_{100} - C_{\text{well}})/(C_{100} - C_o))$. The equation from this linear regression was used to determine an averaged ratio of the normalized intensity at the end of the test to the initial normalized intensity at the start of the test $(C_{T_{t_0+\Delta t}}/C_{T_{t_0}})$. A representative data set and linear regression can be viewed in Figure 2.6. The $C_{T_{t_0+\Delta t}}/C_{T_{t_0}}$ value was used as an input to equation [2.1] developed by Smith (2010). This equation was developed following a mass balance approach on the tracer in the well. The procedure of fitting a linear regression to the normalized intensity data allowed for the calculation of an averaged LNAPL flux through the well over the entire duration of the tracer dilution test.

$$\frac{C_{T_{t_0+\Delta t}}}{C_{T_{t_0}}} = \frac{2\cos\left(\frac{q_{Lw}\Delta t}{2r_w}\right) - \sin\left[2\cos\left(\frac{q_{Lw}\Delta t}{2r_w}\right)\right]}{\pi} \quad [2.1]$$

where q_{Lw} is the flux of LNAPL through the well (L/T), Δt is the length of time of the study (T), and r_w is the radius of the well (L).

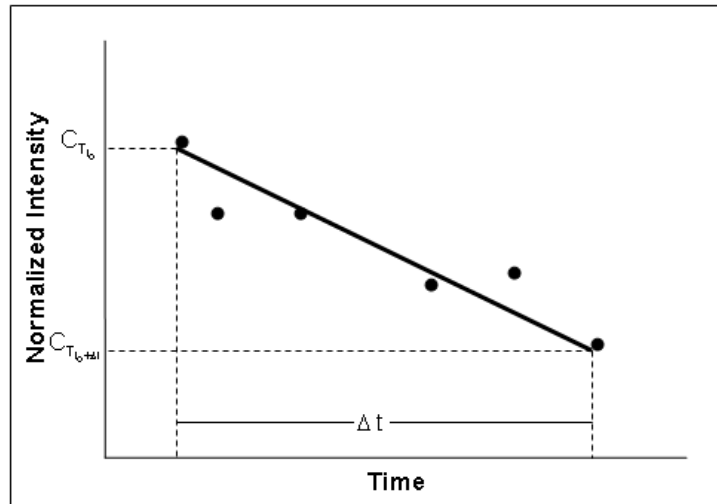


Figure 2.6 - Representative normalized intensity versus time data set with a linear regression.

A critical step in data analysis was to check the accuracy and/or validity of the data. Throughout the duration of the study, a rising water table can influence the flux measurements by forcing the LNAPL with tracer from the well. If the rise is fast enough it will push tracer from the well in a radial direction, leaving LNAPL with tracer in the formation upgradient of the well. This will cause LNAPL with a potentially higher concentration of tracer to migrate back into the well at a later date. For a site experiencing tidal influences it is believed the frequency of the groundwater elevation fluctuations cause an averaging of tracer concentrations between the well and the formation. Consequently, LNAPL upgradient of the well possesses the same tracer concentration of that in the well. As a result decreases in measured tracer concentrations at sites in tidal zones indicate

LNAPL movement. Equation [2.1] was developed based on constant LNAPL thickness in the well. Correspondingly, all data were discarded in which a rise of 0.15 m in the groundwater elevation was observed and/or a 0.15 m change in LNAPL thicknesses in wells. An increase in groundwater elevations and decrease in LNAPL thickness in wells of 0.15 m was determined following observations of increases in tracer concentrations when changes of 0.15 m were observed.

Estimates of the detection limits associated with the methods of the intermittent single well tracer dilution tests were developed. The method detection limits ($\pm q_{Lw}$) are a function of the precision of the intensity measurement (P), the diameter of the well (D) and the time between measurements (Δt).

$$\pm q_{Lw} = \frac{PD}{\Delta t} \quad [2.2]$$

Precision (P) is estimated using the difference between duplicate measurements at C_o , C_{100} , and C_{well} . Measured LNAPL fluxes that are less than the detection limits are reported as less than the observed detection limit.

After checking the input data, results from all valid data sets were compiled (Table 2.1) and analyzed. The range, mean, and median of the measured LNAPL flux values were determined. Relationships between LNAPL thickness in wells, LNAPL specific gravity, distance to the downgradient edge of the body, and LNAPL fluxes were evaluated by plotting the data and performing linear regressions. In all cases the direction of LNAPL flux was assumed to be the same as the direction of groundwater flow. Distances to the downgradient

edge of the continuous LNAPL body were found using the distance of the wells to the downgradient edge of the mapped LNAPL body in the direction of groundwater flow.

The rate of natural losses of the continuous LNAPL bodies was estimated using the following equation:

$$q_{\text{loss}} = \frac{q_{Lw} \bar{b}}{L_{\text{pool}}} \quad [2.3]$$

where q_{loss} is the loss rate in (L/T) to the LNAPL body downgradient of the flux measurement, \bar{b} is the average thickness of hydrocarbon, and L_{pool} is the length (L) to the downgradient edge to the body. Equation [2.3] is derived in Mahler et al. (2010a; pending submission, see the following chapter of this thesis).

2.4 Results and Discussion

Flux measurements, site attributes, and LNAPL properties from the seven sites are presented in Table 2.1. Seven LNAPL fluxes found using tracer dilution tests were dropped due to a decrease in LNAPL thickness or increase in depth to groundwater greater than 0.15 m. LNAPL flux values range from 0.006 to 2.6 m/yr. The mean and median of the LNAPL flux measurements were found to be 0.15 m/yr and 0.064 m/yr, respectively. Ten of the 50 flux measurements were found to be less than the method detection limits. Therefore, they were assigned a value less than the method detection limits. The histogram in Figure 2.7 shows the distribution of the fluxes. The small mean and median show the fluxes of

these bodies are three to five orders of magnitude smaller than typical field measured groundwater fluxes (~100 m/yr).

Table 2.1 - Summary of site data and measured LNAPL flux values (note: < represents less than and N/A represents not applicable).

Site	Well	Soil Type	LNAPL Type	Specific Gravity	LNAPL Thickness (m)	LNAPL Flux (m/yr)	± q _{LW} (m/yr)	Length to Downgradient Pool Edge (m)	Loss Rate (m ³ /ha/yr)
A	1	Silt/Dense Coral Sands	Weathered Diesel	0.8850	1.0229	0.0381	0.0033	227.4510	1.7132
	2	Silt/Dense Coral Sands	Weathered Diesel	0.8850	0.6341	0.0925	0.0180	281.0458	2.0864
	3	Silt/Dense Coral Sands	Weathered Diesel	0.8850	1.2835	0.0309	0.0068	175.1634	2.2631
	4	Silt/Dense Coral Sands	Weathered Diesel	0.8850	1.0564	<0.0067	0.0067	200.0000	0.3489
	5	Silt/Dense Coral Sands	Weathered Diesel	0.8850	0.3826	0.0472	0.0193	23.5294	7.6720
B	1	Glacial Till	Railroad Diesel	0.8771	0.0579	0.0247	0.0017	40.0000	0.3570
	2	Glacial Till	Railroad Diesel	0.9343	0.3659	0.0430	0.0029	120.0000	1.3119
	3	Glacial Till	Railroad Diesel	0.8813	0.0762	0.0474	0.0019	230.0000	0.1570
	4	Glacial Till	Railroad Diesel		0.0549	0.0640	0.0041	117.5000	0.2988
	5	Glacial Till	Railroad Diesel	0.8854	0.5671	0.0318	0.0067	125.0000	1.4408
C	1	Sand with Gravel	Railroad Diesel	0.9206	0.1535	<0.0065	0.0065	589.3805	0.0170
	2	Sand with Gravel	Railroad Diesel	0.9206	0.1250	<0.0065	0.0065	488.4956	0.0167
	3	Sand with Gravel	Railroad Diesel	0.9206	0.1169	<0.0065	0.0065	454.8673	0.0167
	4	Sand, Gravel, Cobbles	Railroad Diesel	0.9206	0.3953			442.4779	
	5	Sand with Gravel	Railroad Diesel	0.9206	0.2195	<0.0128	0.0128	353.9823	0.0794
	6	Gravel, Cobbles	Railroad Diesel	0.9206	0.2734			395.5752	
	7	Gravel, Cobbles	Railroad Diesel	0.9206	0.2937			315.0442	
	8	Sand with Silt	Railroad Diesel	0.9206	0.2978	<0.0064	0.0064	205.3097	0.0929
	9	sand	Railroad Diesel	0.9206	0.2957	0.1142	0.0064	53.0973	6.3613
	10	Sand with Silt	Railroad Diesel	0.9206	0.2947	0.0659	0.0064	49.5575	3.9206
D	1	Fine Sand	Gasoline	0.8012	0.4797	0.0644	0.0109	14.1303	21.8528
	2	Fine Sand	Gasoline	0.8111	1.4024	0.0321	0.0064	37.7622	11.9078
	3	Fine Sand	Gasoline	0.8194	0.6992	0.1551	0.0066	83.9161	12.9238
	4	Fine Sand	Gasoline	0.8133	0.1745	0.1284	0.0063	138.4615	1.6185
	5	Fine Sand	Gasoline		0.1514	0.2325	0.0143	12.5602	28.0317
	6	Fine Sand	Gasoline		0.1931	0.0883	0.0191	22.7654	7.4861
	7	Fine Sand	Gasoline	0.8108	0.5539	<0.0225	0.0225	32.9706	3.7865
	8	Fine Sand	Gasoline	0.8552	0.5112	0.0632	0.0030	16.4853	19.6023
	9	Fine Sand	Gasoline	0.8081	0.8089	0.2457	0.0082	92.3077	21.5346
	10	Fine Sand	Gasoline	0.8448	0.7378	0.0285	0.0067	12.5602	16.7437
	11	Fine Sand	Gasoline	0.8294	0.0945	0.1279	0.0030	125.8741	0.9600
	12	Fine Sand	Gasoline	0.8206	1.2182			39.8601	
	13	Fine Sand	Gasoline		1.0838	2.5627	2.5627	46.1538	601.8127
	14	Fine Sand	Gasoline	0.8543	0.5452	0.3231	0.0066	92.3077	19.0865
	15	Fine Sand	Gasoline	0.8476	0.4741	0.1752	0.0060	15.7003	52.8979
	16	Fine Sand	Gasoline	0.8458	0.3669	0.0813	0.0065	29.3706	10.1600
	17	Fine Sand	Gasoline	0.8561	0.6966	0.1212	0.0132	67.1329	12.5727
	18	Fine Sand	Gasoline	0.8159	0.2482	0.2484	0.0055	58.7413	10.4979
	19	Fine Sand	Gasoline		0.5188	0.2284	0.0030	12.5602	94.3223
	20	Fine Sand	Gasoline	0.8198	0.5030	0.3293	0.0133	71.3287	23.2216
	21	Fine Sand	Gasoline	0.8101	0.9167			77.6224	
	22	Fine Sand	Gasoline	0.8717	0.5356	0.0984	0.0166	33.5664	15.6970
	23	Fine Sand	Gasoline	0.8007	0.1189				
E	1	Silty Clay	Fuel Oil	0.9219	1.4634			17.7515	
	2	Silty Clay	Fuel Oil	0.9219	0.6250	<0.0711	0.0711	27.2189	16.3208
	3	Silty Clay	Fuel Oil	0.9219	0.6098	<0.009	0.0090	114.7929	0.4783
	4	Silty Clay	Fuel Oil	0.9219	1.4665	<0.0064	0.0064	15.3846	6.0722
	5	Silty Clay	Fuel Oil	0.9219	1.0427	<0.0158	0.0158	5.9172	27.8065
	6	Silty Clay	Fuel Oil	0.9219	1.2195	<0.0331	0.0331	23.6686	17.0719
F	1	Sand	Diesel	0.7836	0.4512	0.0101	N/A	39.4161	1.1517
	2	Sand	Kerosene	0.7836	0.2348	0.0280	N/A	344.5255	0.1911
	3	Sand	Mixture	0.8449	0.1738	0.2027	N/A	192.7007	1.8284
	4	Sand	Mixture	0.8177	0.2043	0.0643	N/A	143.0657	0.9185
	5	Sand	Mixture	0.8154	0.2927	0.5832	N/A	26.2774	64.9616
	6	Sand	Mixture	0.8694	0.1738	0.0756	N/A	153.2847	0.8572
	7	Sand or silt	Mixture	0.9023	0.5488	0.4787	N/A		
G		Sand	Lube Oil		0.1439	0.0593			

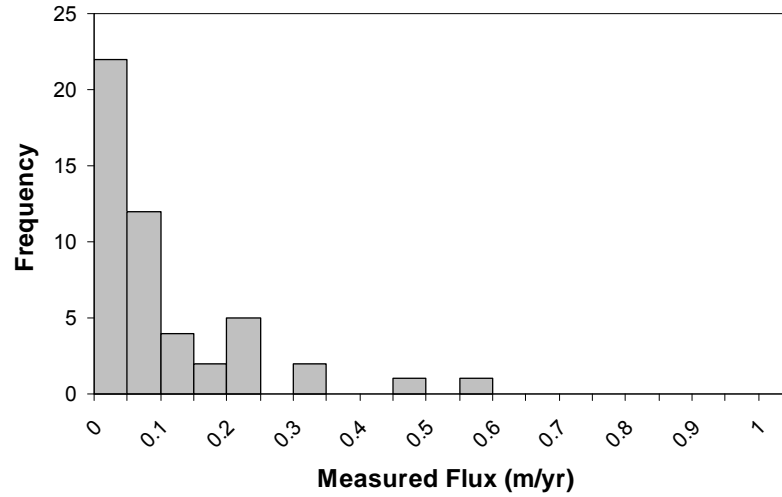


Figure 2.7 - Histogram of the measured fluxes at the seven sites.

Figure 2.8 plots LNAPL flux versus LNAPL thickness in the well. A linear regression of the data was performed. The value of LNAPL flux is largely independent of LNAPL thickness in the well, following the linear regressions. The lack of correlation and small slopes of the linear regressions suggest a change in LNAPL well thickness has a very small impact on LNAPL fluxes, if any.

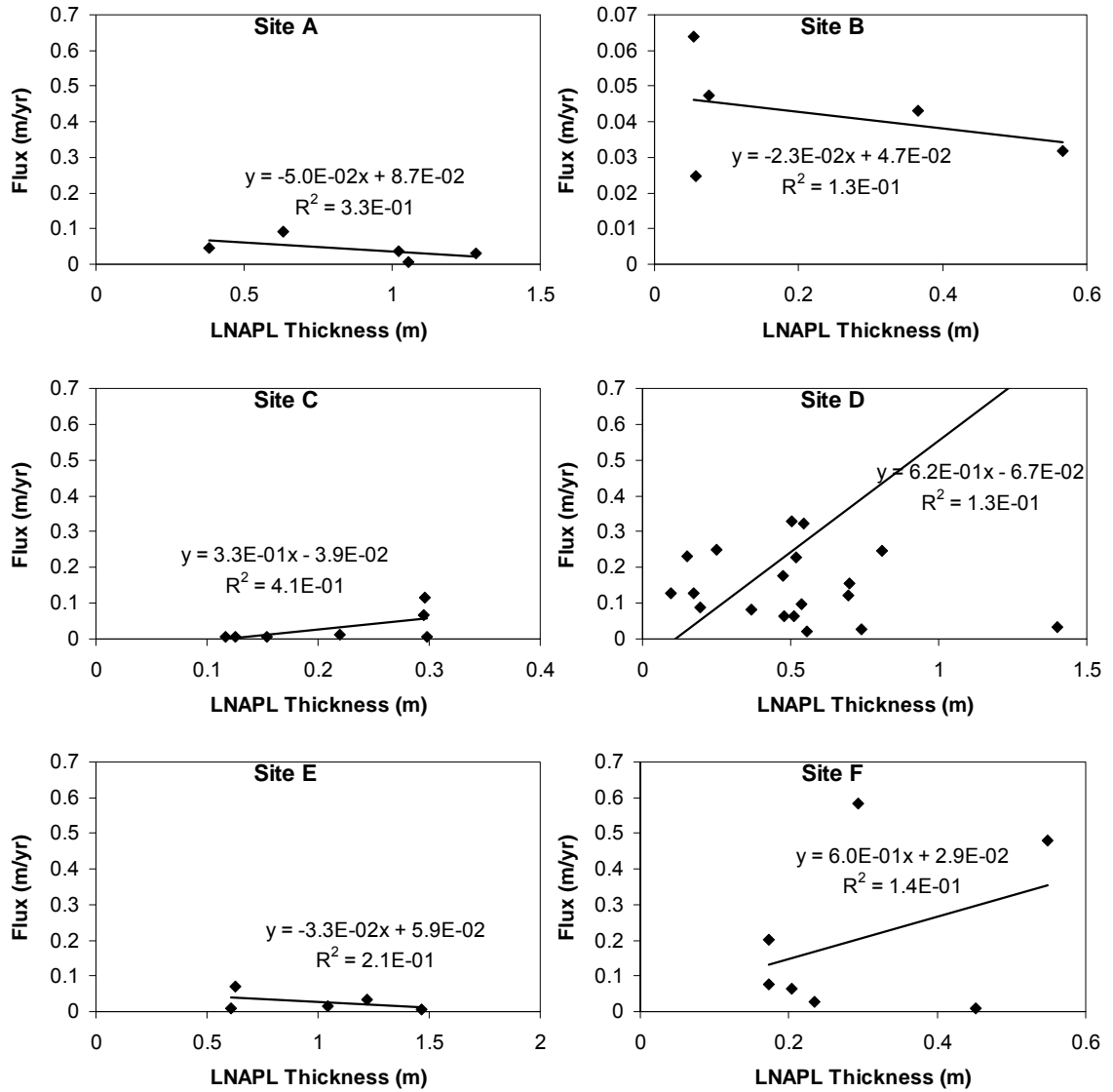


Figure 2.8 - Comparison of LNAPL thickness in wells to LNAPL fluxes for sites A-F.

The influence of specific gravity of LNAPL on fluxes is evaluated in Figure 2.9. The data from the sites were compiled into one graph to evaluate the lighter and heavier LNAPLs present at the different sites. It has been hypothesized heavier end LNAPLs likely encounter more resistance to flow compared to lighter end LNAPLs. However, this was not observed in the data.

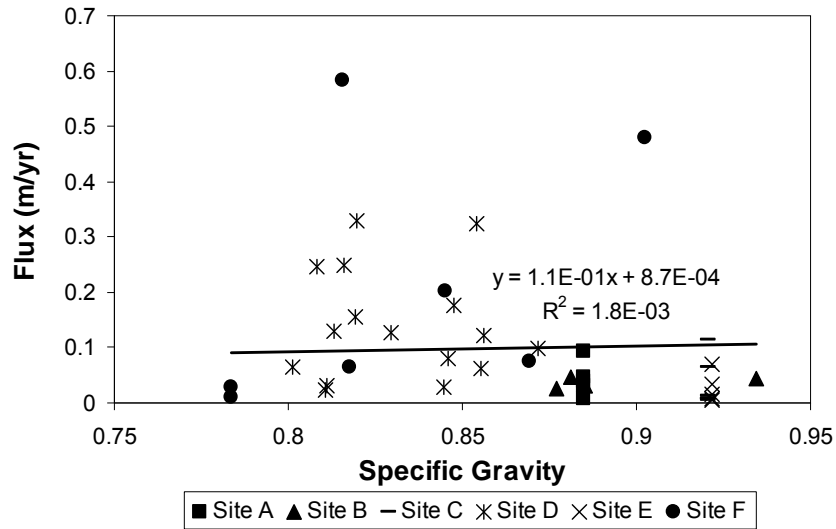


Figure 2.9 - Specific gravity of LNAPL at sites A-F plotted against LNAPL flux.

Fluxes were also compared to the length to the downgradient edge of the LNAPL body. This is shown in Figure 2.10. There does not appear to be a correlation between these parameters. As discussed in the Mahler et al. (2010a; pending submission, see the following chapter of this thesis), if these bodies possess an active source, a relationship between the magnitude of LNAPL flux and the length to the downgradient edge of the body would be observed. Sources of LNAPL at all these sites are believed to be removed. The absence of sources and no correlation between flux and the length to downgradient LNAPL body edge could be indicative of a stable or shrinking LNAPL bodies. In a stable body the internally measured LNAPL fluxes could be a result of redistribution of LNAPL, rather than the overall migration of the LNAPL body.

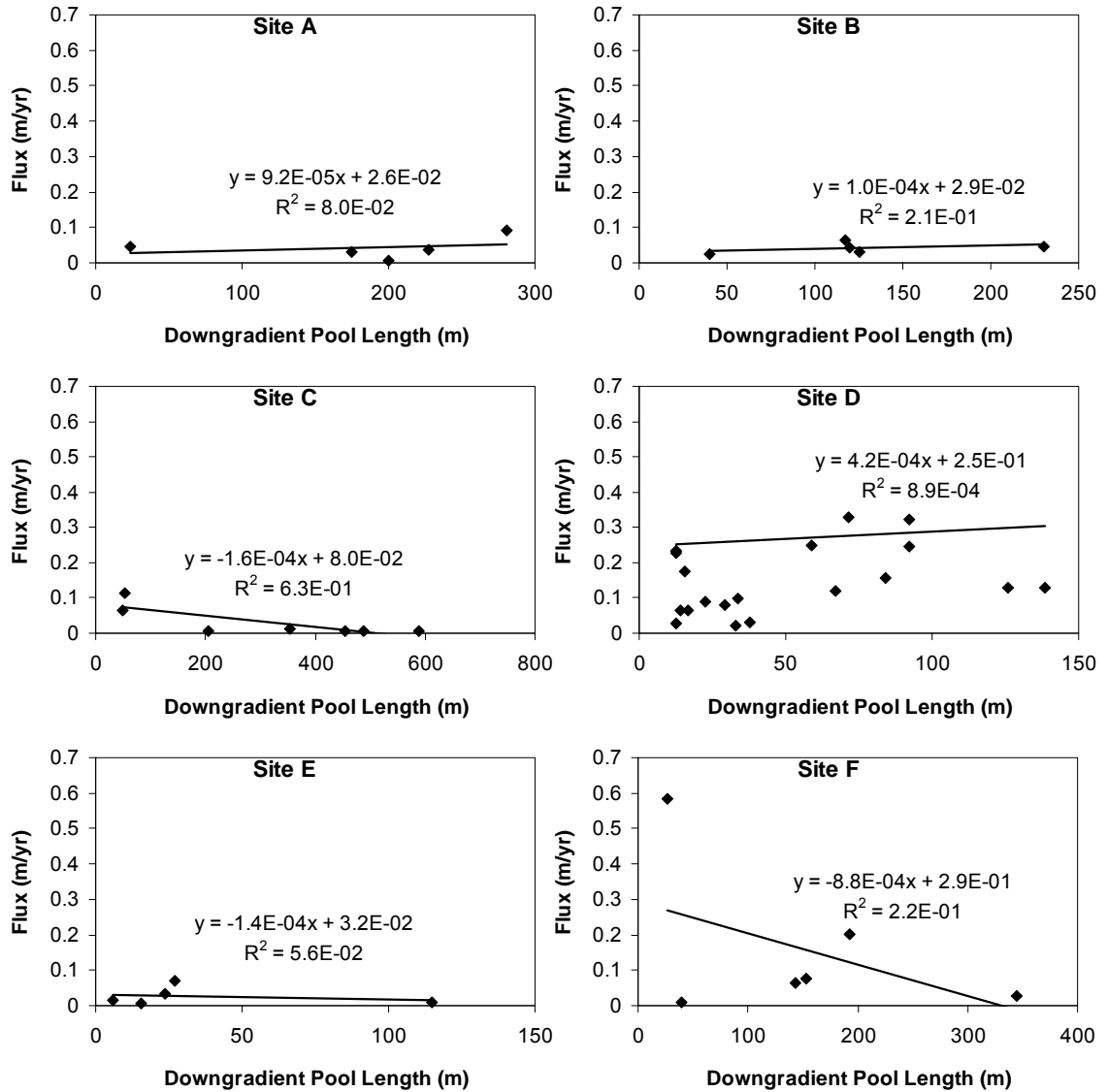


Figure 2.10 - A presentation of the relationship between the length to the downgradient pool edge and LNAPL flux.

Assuming that the LNAPL bodies are stable equation [2.3] was used to estimate the loss rates to the downgradient LNAPL bodies. The distribution of the calculated loss rates are presented in Figure 2.11. The mean and median of the calculated loss rates were found to be 24.0 m³/ha/yr and 5.0 m³/ha/yr, respectively. A third of the calculated loss rates fall within the range found by Lundegard and Johnson (2006) of 1.25 to 12.5 m³/ha/yr. More than a

third of the loss rates were found to be greater than this range. The remaining loss rates fall below this range. Care needs to be taken when interpreting the loss rates due to the limitations of equation [2.3] and the lack of relationship between the flux and the length to the downgradient edge of the LNAPL body. However, the loss rates found here provide an estimate of potential loss rates the LNAPL bodies may be experiencing.

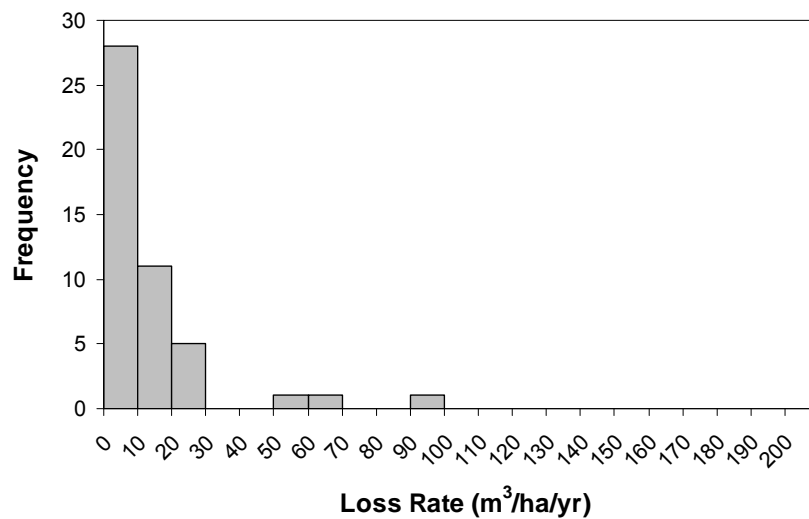


Figure 2.11 - Histogram showing the distribution of calculated loss rates to the LNAPL bodies assuming the bodies are stable.

2.5 Conclusions

Single well tracer dilution techniques have been used at seven sites to determine LNAPL fluxes in 50 wells. This paper shows that LNAPL fluxes are on the order of tenths to hundredths of meters per year. This is three to five orders of magnitude less than typical groundwater fluxes. The small measured LNAPL fluxes could imply the bodies evaluated are stable or shrinking. Sources to the LNAPL bodies are believed to have been removed. This could explain the lack

of correlation between the length to the downgradient edge and LNAPL fluxes. The majority of calculated loss rates fall within or above the range found by Lundegard and Johnson (2006). The current practice of using LNAPL thickness in wells as a gauge for LNAPL stability seems invalid based on the absence of a relationship between LNAPL fluxes and LNAPL thicknesses in wells and lengths to the downgradient edge of the body. A more representative performance metric is needed to better evaluate the stability of these bodies. Fluxes within these bodies and rates of natural LNAPL losses could be used as a metric for LNAPL stability.

Assumptions made in the development of single well tracer dilution techniques used for measuring LNAPL fluxes limit its application. Falling water tables would result in flux measurements larger than actual fluxes. This would be due to LNAPL from the formation moving into the well and diluting the tracer concentrations in the well. Rising water tables could force LNAPL with tracer from the well into the formation. At a later date the LNAPL with tracer in the formation can return to the well and potentially increase tracer concentrations in the well. Future work is still needed in quantifying the effects and eliminating the problems with measuring LNAPL fluxes under conditions of changing groundwater elevations. Even with these limitations conservative LNAPL fluxes can still be determined.

2.6 Acknowledgements

Funding for the field studies described herein was provided by Chevron, BP, CSX Transportation Inc., and Union Pacific Railroad. Field data was collected with support from Tri-Hydro Corp., AECOM Technology Corp., URS Corp., Stantec Inc., Arcadis, and CH2M Hill.

3 A Mass Balance Approach to Resolving LNAPL Stability

3.1 Abstract

Petroleum liquids in shallow subsurface settings are referred to as light non-aqueous phase liquids (LNAPLs). A primary concern with continuous bodies of LNAPL is their potential to expand or translate laterally. Flux measurements made on continuous LNAPL bodies typically result in non-zero values. These fluxes are measured internal to the body and are commonly extrapolated to the edges of the pools. However, many LNAPL bodies have been observed to be stable for long time periods. This observed stability of LNAPL bodies could be due to downgradient natural losses balancing non-zero upgradient LNAPL fluxes. This paper examines the influence of natural losses on stability of LNAPL bodies. A proof-of-concept sand tank experiment was conducted. Methyl tert-butyl ether (MTBE) was injected into a sand at five constant injection rates. The MTBE body initially expanded relatively quickly, the expansion slowed and stopped for each of the steady injection systems. Analytical models were also developed to aid in the description of this process. Three geometries were considered (one-dimensional, circular, and oblong). The models developed to examine the extent of the LNAPL body through time show that the extent of the body approaches a finite steady-state extent over time. By varying the loss rate it was found that the time for a body to become stable is more dramatically affected than varying the

LNAPL source release rate. The models developed to investigate the distributions of LNAPL flux throughout the body show that with a constant release, non-zero fluxes, internal to the stable LNAPL body, exist. From this, it is believed that losses play an fundamental role in the stabilization of LNAPL bodies.

3.2 Introduction

Past industrial practices have resulted in accumulation of light non-aqueous phase liquid (LNAPL) bodies beneath petroleum facilities. A primary concern with LNAPL bodies is their potential to expand or translate laterally. Methods used to resolve the stability of LNAPL bodies have largely focused on point measurements of LNAPL flux internal to bodies of continuous LNAPL. Estimates of LNAPL flux can be developed using the formation conductivity to LNAPL, estimates of the LNAPL head gradient, and Darcy's equation. Alternatively, Taylor (2004); Sale et al. (2007a; 2007b); Smith (2008); and Smith et al. (2010) describe the use of single well tracer dilution techniques to resolve LNAPL flux. Common to these methods small LNAPL fluxes are measured internal to the LNAPL body (Sale, 2003 and Mahler et al., 2010b, see Chapter 2 of this thesis). These fluxes have led to concerns that LNAPL bodies are expanding and/or translating laterally, albeit slowly.

In contrast, groundwater plumes downgradient of LNAPL bodies have commonly been shown to be stable or shrinking (e.g. Weidemeir et al., 1999). The observed stability of dissolved plumes downgradient from LNAPL bodies has

been attributed to biologically mediated losses of the dissolved phase LNAPL constituents. Concurrent movement of LNAPL and stable downgradient plumes present an apparent contradiction. A possible reconciliation of the two perspectives is that LNAPL losses (via evaporation and dissolution) are controlling the stability of LNAPL bodies. In this way, LNAPL bodies are like dissolved hydrocarbon plumes; internal fluxes and the extent of LNAPL bodies are controlled by naturally occurring losses. Processes governing natural losses of LNAPL (evaporation and dissolution) and the magnitudes of the losses, are reviewed in Abranovic et al. (2001), Held and Celia (2001), Chaplin et al. (2002), Pasteris et al. (2002), Anwar et al. (2003), Harper et al. (2003), Kim and Corapcioglu (2003), Amos et al. (2005), Johnson et al. (2006), Lundegard and Johnson (2006), Eweis et al. (2007), and ITRC (2009). Based on natural loss rates found by Lundegard and Johnson (2006), magnitudes of LNAPL losses range from 1.25 to 12.5 m³/ha/yr (based on an LNAPL density of 0.8 g/cm³).

The objective of this paper is to evaluate the impacts of natural losses of LNAPL on the stability of LNAPL bodies using a mass balance method. As a first step, a proof-of-concept experiment is presented. Methyl tert-butyl ether (MTBE) was added to a sand tank at constant rates that were increased in a step-wise manner. The MTBE body was exposed to losses due to dissolution and evaporation and the expansion of the body was observed over time. Secondly, mass balances were employed to develop analytical solutions for three idealized LNAPL body geometries (one-dimensional, circular, and oblong). One set of solutions describe the extent of LNAPL bodies as a function of LNAPL

inflow, rates of natural losses, and time. A second set of analytical solutions describe LNAPL fluxes as a function of position, LNAPL inflow, and rates of natural losses. Next, the analytical solutions are employed to explore the sensitivity of the results to key inputs. Lastly, conclusions are presented highlighting the observation that LNAPL losses can play an important role in governing the overall stability of LNAPL bodies.

3.3 Laboratory Study

The objective of the laboratory study was to determine if natural losses can control the stability of LNAPL bodies. Furthermore, results are used in the subsequent section to test analytical solutions advanced in the following section.

3.3.1 Materials and Methods

A two-dimensional sand tank was employed to simulate an aquifer. The internal dimensions of the tank were 92.2 cm long, 47.5 cm high, and 2.54 cm wide. One side of the tank was composed of glass. All other internal surfaces were stainless steel. The top of the tank was open and exposed to the atmosphere. The tank was filled with a quartz sand (UNIMIN 4095; Target Products LTD, Burnaby, BC, Canada). Physical properties of the sand, found by PTS Laboratories Inc. (Santa Fe Springs, CA) and presented in Iltis (2007), are presented in Table 3.1. UNIMIN 4095 is a fine to medium grained sand with 95% retained on a number 40 sieve. The sand was rained into the tank such that a

uniform packing was achieved. The calculated porosity of the packed sand in the sand tank was 0.426.

Table 3.1 - Porous media parameters.

Soil Sample ID	UNIMIN 4095	
Grain Size Description	ASTM-USCS Scale	Medium Sand
Mean Grain Size	mm	0.833
Porosity	%	44.5
Specific Permeability to Air	millidarcy	7360
Permeability to Water	millidarcy	2697
Saturated Hydraulic Conductivity	cm/sec	0.00266
Bulk Density	g/cm ³	1.46
Grain Density	g/cm ³	2.63

The tank was filled with de-aired Fort Collins, Colorado tap water and flushed for approximately 2 days to remove trapped gasses. Head in the inflow tank was held constant using a Mariott siphon. A constant flow of water through the tank was sustained by pumping water out of the effluent head tank using a peristaltic pump (ISMATEC SA, Glattbrugg, Switzerland). The effluent line from the sand tank was equipped with a glass 20 mL in-line sampling vial used for collecting effluent water sample concentration measurements. The experimental setup is presented in Figure 3.1.

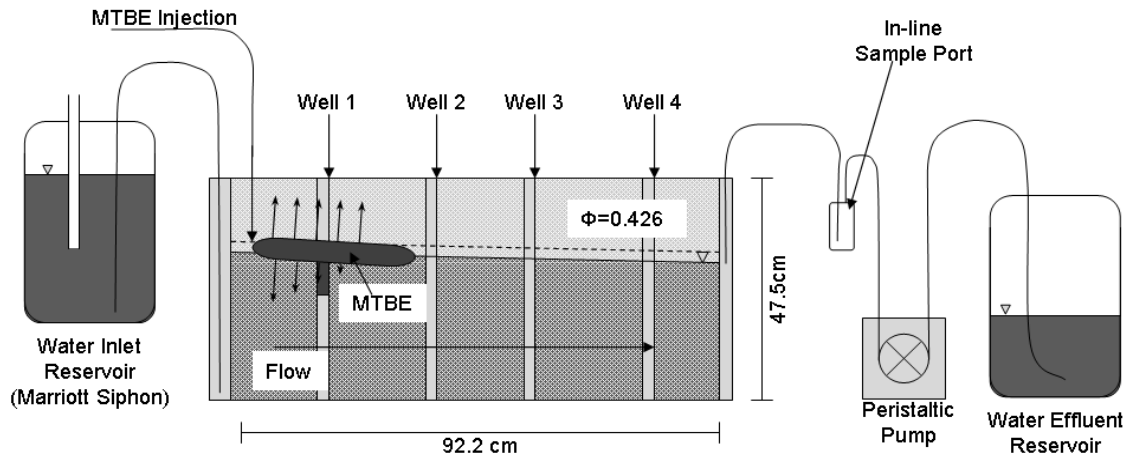


Figure 3.1 - Experimental setup for evaluating the expansion on an LNAPL body with a constant source.

Water levels were lowered to create a 13 cm vadose zone and the water flow rate was set to 0.64 mL/min. This produced a water seepage velocity of 0.25 m/day. Subsequently, methyl tert-butyl ether (MTBE; OmniSolv, Darmstadt, Germany) dyed red with 2.5 mg/L Sudan IV (Aldrich) was manually injected into the sand tank using a syringe. The MTBE was injected from the syringe into the tank over a period of 2-5 minutes on a daily basis. Efforts to continuously deliver the MTBE to the tank were unsuccessful. Two challenges to establishing a continuous MTBE feed were the low flow rates and the high vapor pressure of MTBE. The combination of these two conditions led to formation of gas bubbles in the feed lines that caused the injection rate to be erratic. Initially the injection of MTBE occurred below the water table at rates of 9 and 15 mL/day followed by injections above the water table at rates of 15, 40, 120, and 200 mL/day. In total six different injection systems were examined in which MTBE was injected both above and below the water table.

Once the length of the MTBE body and its dissolved concentrations appeared to stabilize the rate of MTBE addition was increased. Samples of effluent water from the tank were obtained from the in-line water sampling vessel on a daily basis. Concentrations of MTBE were measured using an HP 5890A gas chromatograph (Hewlett-Packard Co., Avondale, Pennsylvania) equipped with a flame ionizing detector (FID) and a RTX-5022 column (Restek Corp., Bellefonte, PA). The water samples were capped and stored at 8.5° C. All samples were analyzed within 14 days of their collection.

3.3.2 Results and Discussion

For all the injection rates an initial expansion, followed by a decrease in the rate of expansion and ultimately, a stable length of the MTBE body was observed. A plot of the MTBE body length as a function of time and MTBE inflow is presented in Figure 3.2.

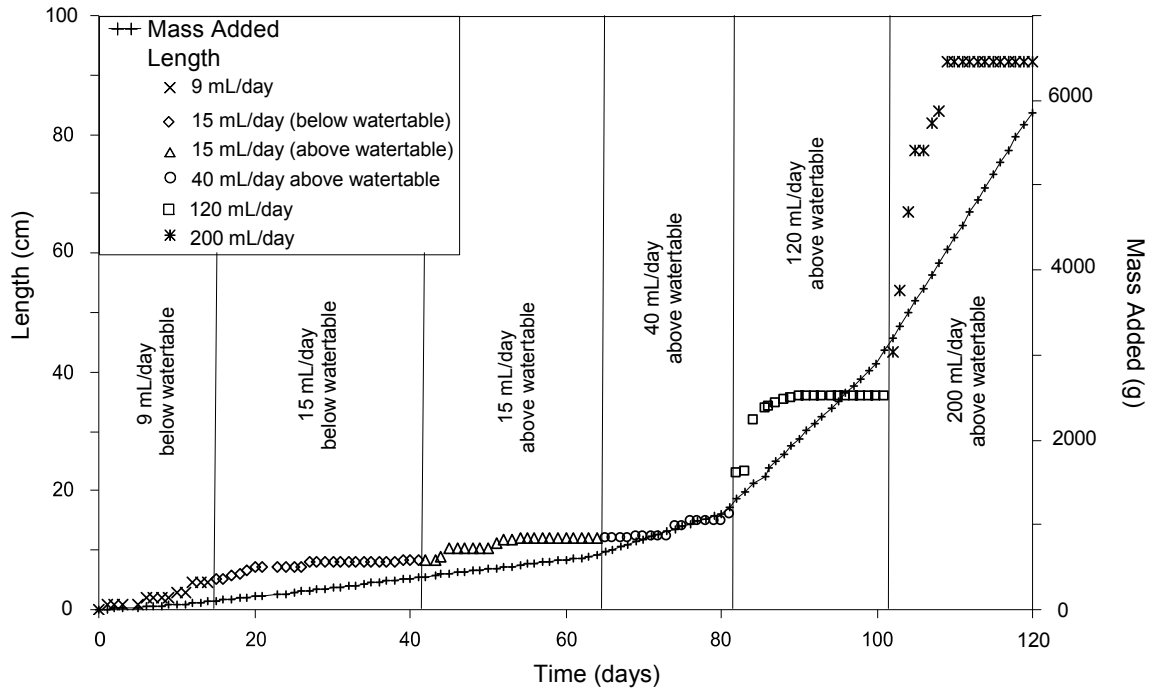


Figure 3.2 - Expansion of the continuous MTBE body exposed to losses due to dissolution and evaporation.

The steady-state MTBE lengths at each injection location and rate are given in Table 3.2. At steady-state the MTBE extent and dissolved concentrations in the effluent samples were stable.

Table 3.2 - Steady-state injection length at each injection location and rate.

Injection Location	Injection Rate	Steady-State Length
	(mL/day)	(m)
Below WT	9	0.0471
Below WT	15	0.085
Above WT	15	0.012
Above WT	40	0.151
Above WT	120	0.36
Above WT	200	0.922

Regression analysis was performed using the MTBE length versus time data for the 15, 40, 120, and 200 mL/day injection rates in which the injection location was situated above the water table (Figure 3.3). A best fit logarithmic trend line was developed using Microsoft Excel®. The derivatives of the

logarithmic best fit trend lines were used to determine how rapidly the MTBE body expansion ceased. Figure 3.4 shows that in all cases the initial rate of change in the length of the body occurred quickly and then asymptotically approaches zero.

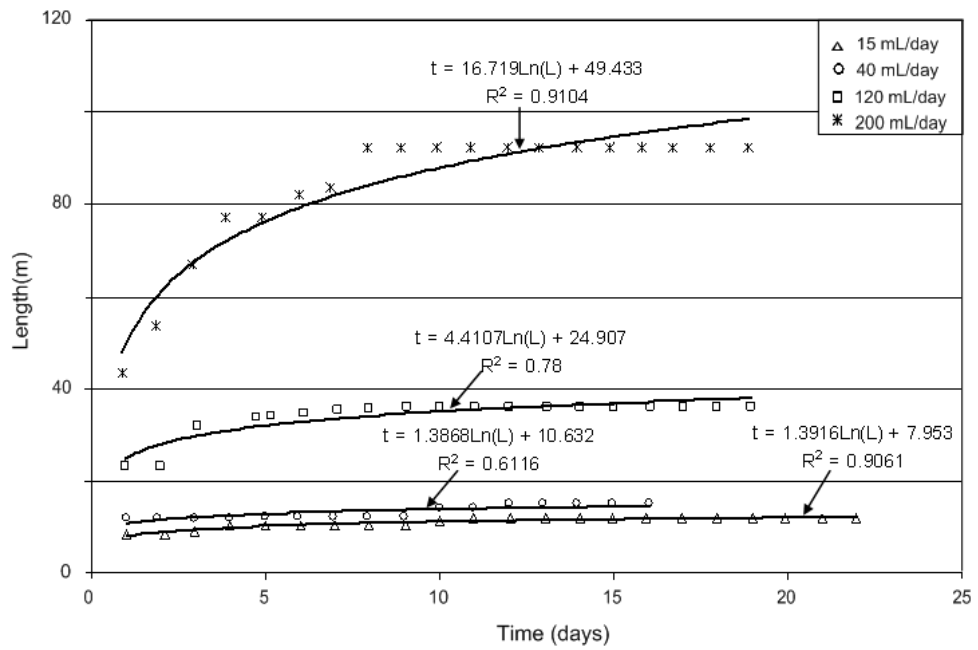


Figure 3.3 - Best fit logarithmic trend lines for the MTBE length versus time.

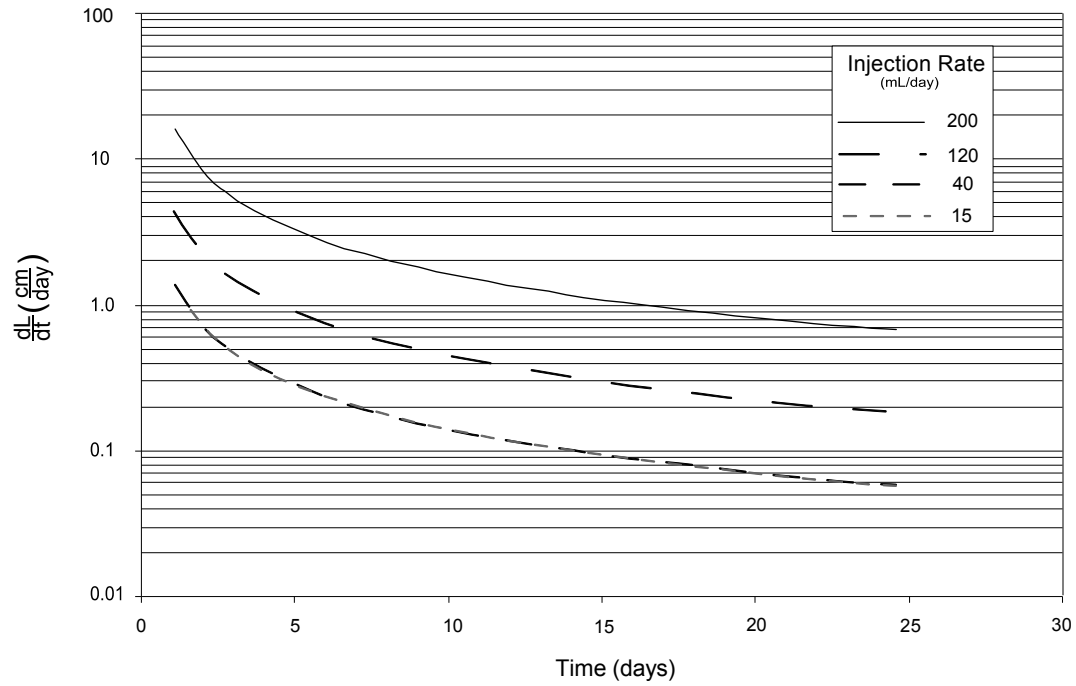


Figure 3.4 - Rate of change of the length of the MTBE body versus time.

When the body was determined to be stable a mass balance on the entire system was performed in order to determine the loss rate of the MTBE due to evaporation (Evaporation = Inflow – Dissolution). This mass balance can be observed in Figure 3.5 in which the shaded regions indicate steady-state. The dissolution and evaporation loss rates are presented in Table 3.3.

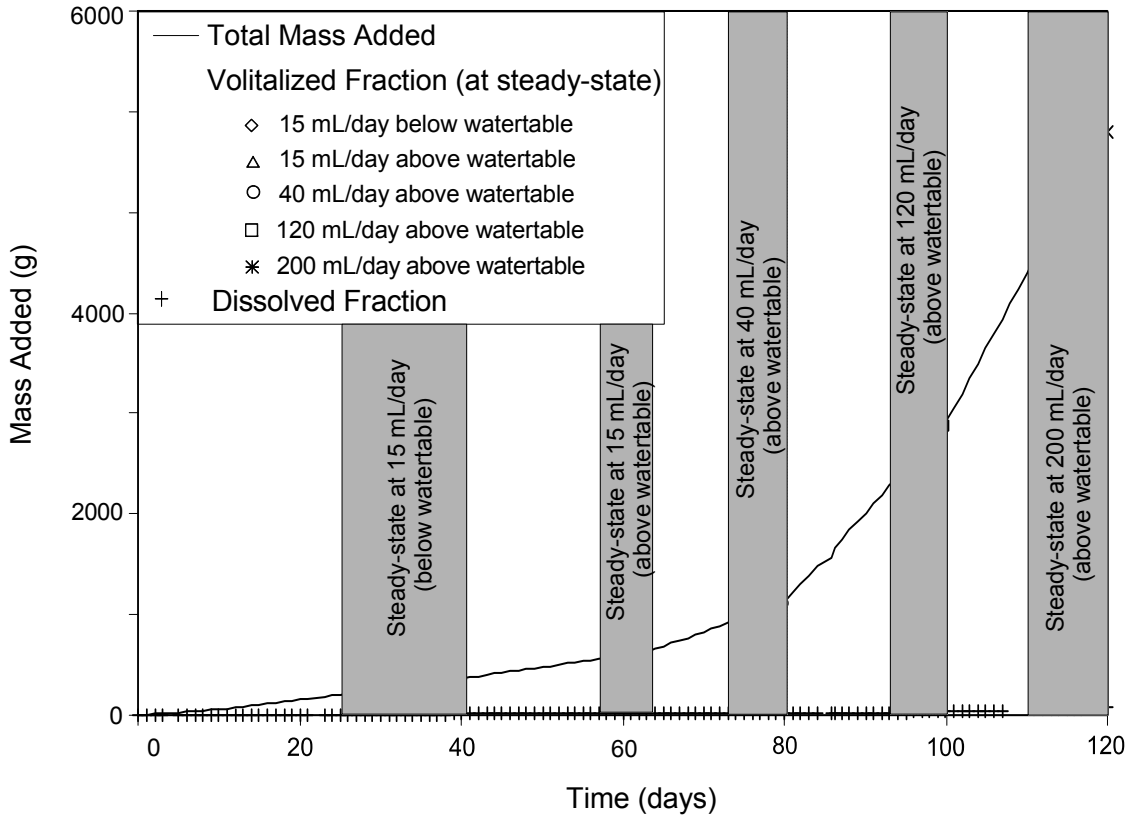


Figure 3.5 - Mass balance performed to determine the relative influence of dissolution and evaporation on the stability of the MTBE body.

Table 3.3 - Loss rates due to evaporation and dissolution.

Injection Location	Injection Rate	Dissolution Loss Rate	Evaporation Loss Rate	Mass Lost Ratio
	(mL/day)	(m ³ /ha/yr)	(m ³ /ha/yr)	
Below WT	15	885	25500	28.8:1
Above WT	15	262	17700	67.6:1
Above WT	40	255	37800	148:1
Above WT	120	508	47400	93.3:1
Above WT	200	396	30800	77.8:1

The loss rates due to evaporation are one to two orders of magnitude greater than dissolution, indicating that evaporation is mainly controlling the stability of the MTBE body. From this observation, the partial pressure and solubility of common petroleum liquids could be critical parameters for evaluating the influence of losses on the stabilization of an LNAPL body. Boiling points and

relative persistence data for common petroleum liquids are summarized in Table 3.4.

Table 3.4 - Boiling point and relative persistence data for common LNAPLs (Scholz et al., 1999).

LNAPL Type	Specific Gravity	Boiling point	Relative persistence
		(°C)	
Gasoline	0.73 to 0.74	40 to 150	1
Jet Fuel (JP-4)	0.75 to 0.80	95 to 270	~2
Kerosene	0.80 to 0.88	200 to 300	NA
Fuel Oil No. 2 (Diesel)	0.88	33.9 to 185	8
Lube Oil (Crankcase)	0.87	376.7 to 438.9	~55
Kuwait Light Crude Oil	0.83	NA	~320
Fuel Oil No. 6 (Bunker)	0.96 to 0.97	323.9 to 441.1	400
North Slope Crude Oil	0.89	NA	~450
San Ardo (CA) Crude Oil	0.99	NA	~590
Residual Asphaltene	--	>400	1600

Lundegard and Johnson (2006) describe loss rates at a field site ranging from approximately 1.25 to 12.5 m³/ha/yr. The large difference between the loss rates in this experiment and those in the field is likely due to the large solubility and partial pressures of MTBE, as well as the small vadose zone in the sand tank experiment.

3.4 Theory

The following advances a mass balance approach for estimating the areal extent of continuous LNAPL bodies as a function of upgradient LNAPL flux (inflow) and downgradient LNAPL dissolution and evaporation (losses). Results provide a basis for estimating the extent of a continuous LNAPL body as a function of time, LNAPL inflow, and rates of natural losses. Three geometries

were considered. These include a one-dimensional LNAPL body parallel to LNAPL flow, a circular LNAPL body, and an oblong LNAPL body composed of an upgradient half circle tied to a downgradient half ellipse. These geometries are illustrated in cross-section and plan view in Figure 3.6.

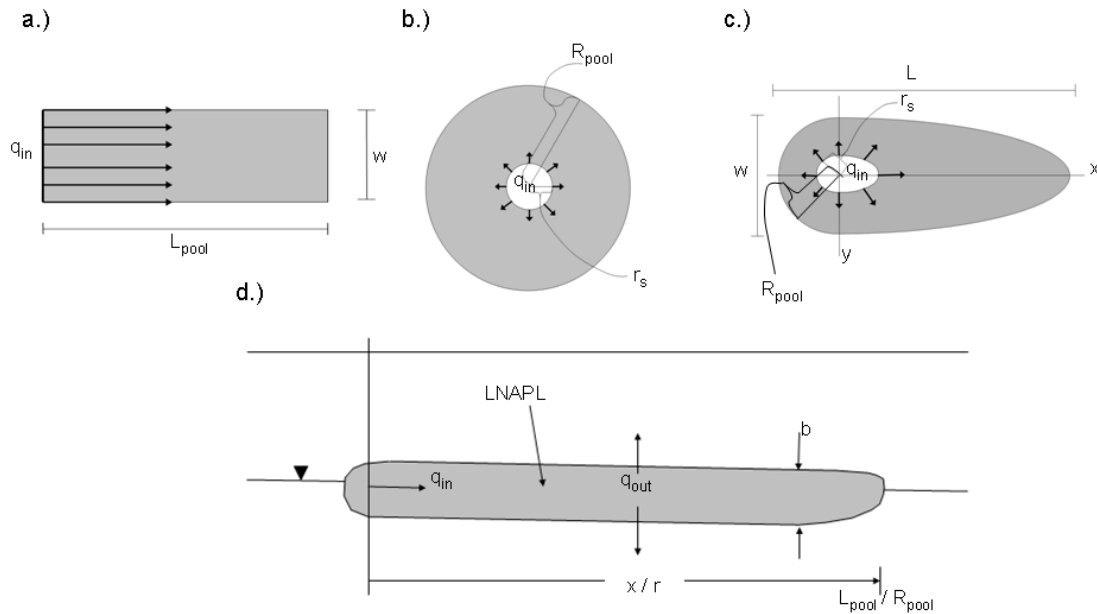


Figure 3.6 - Conceptual basis for mass balance. The a.) one-dimensional, b.) circular, and c.) oblong geometries are shown, as well as the d.) cross-sectional view associated with all three geometries.

3.4.1 Extent

One-Dimensional – A mass balance was performed on an LNAPL body through a uniform LNAPL flow field as a whole to develop solutions of LNAPL extent versus time. Panels a and d in Figure 3.6 show the one-dimensional plan and cross-sectional views for the one-dimensional scenario. Balancing inflow and outflow:

$$\frac{dM_{\text{Total}}}{dt} = q_{\text{in}} \rho A_{\text{in}} - q_{\text{out}} \rho A_{\text{out}} \quad [3.1]$$

where M_{Total} is the total mass (M) of continuous LNAPL, t is time (T), q_{in} is the upgradient volumetric flux of LNAPL (L/T), q_{out} is the volumetric flux of LNAPL out of the system due to losses (L/T), ρ is the LNAPL density (M/L³), A_{in} is the cross-sectional area normal to LNAPL inflow (L²), A_{out} is the cross-sectional area normal to LNAPL outflow (L²). A'_{out} is the surface area exposed to natural losses.

The total mass, inflow area, and outflow area are defined in equations [3.2-3.4].

$$M_{\text{Total}} = \rho S \phi b A_{\text{out}} \quad [3.2]$$

$$A'_{\text{in}} = b \quad [3.3]$$

$$A'_{\text{out}} = x \quad [3.4]$$

where S is the average LNAPL saturation in the body of continuous LNAPL (unitless), ϕ is the porosity of the porous media (unitless), b is the formation thickness of the continuous LNAPL body (L). A'_{in} and A'_{out} are the areas normal to inflow and outflow, respectively, per unit width (w) of LNAPL (L). As shown in [3.3] and [3.4] A'_{in} and A'_{out} are equated to b and the downgradient length of the continuous LNAPL pool, x (L).

Substituting [3.2-3.4] into [3.1], separating the variables, and integrating yields:

$$\int_0^{L_{\text{pool}}(t)} \frac{\rho S \phi b d(x)}{q_{\text{in}} \rho b - q_{\text{out}} \rho x} = \int_0^t dt \quad [3.5]$$

where L_{pool} (L) is the length of the LNAPL body at time t. Assuming that ρ , S, ϕ , and b are constant, the solution to [3.5] is:

$$L_{\text{pool}}(t) = \frac{q_{\text{in}} b}{q_{\text{out}}} \left(1 - e^{-\frac{q_{\text{out}} t}{S \phi b}} \right) \quad [3.6]$$

At large time [3.6] simplifies to:

$$L_{\text{pool}} = \frac{q_{\text{in}} b}{q_{\text{out}}} \quad [3.7]$$

Circular – The same methods are employed for a circular LNAPL body.

In this case the cross-sectional area perpendicular to LNAPL inflow (A_{in}) and the surface area of the continuous LNAPL body exposed to losses (A_{out}) are:

$$A_{\text{in}} = b 2\pi r_s \quad [3.8]$$

$$A_{\text{out}} = \pi R_{\text{pool}}^2 \quad [3.9]$$

where R_{pool} is the radial extent of the LNAPL body (L) and r_s is the radius of the source (L). This is shown in panel b of Figure 3.6. Following the steps outlined above:

$$R_{\text{pool}} = \sqrt{\frac{(2r_s b q_{\text{in}} + r_s^2 q_{\text{out}})}{q_{\text{out}}} \left(1 - e^{-\frac{q_{\text{out}} t}{S \phi b}} \right)} \quad [3.10]$$

and at large time:

$$R_{\text{pool}} = \sqrt{\frac{(2r_s b q_{\text{in}} + r_s^2 q_{\text{out}})}{q_{\text{out}}}} \quad [3.11]$$

Equations [3.10] and [3.11] are most appropriate for the conditions of point or circular sources where the gradient through the LNAPL body due to the release is large relative to the gradient of the groundwater.

Oblong – Observed shapes of continuous LNAPL bodies are often not circular. As a first step in evaluating this scenario the circular extent versus time (equation [3.10]) is converted to Cartesian coordinates. Estimates of the length to width ratio of the LNAPL body were integrated into the circular solution and the following oblong solution was derived.

$$x = \begin{cases} a \sqrt{\frac{(2r_s b q_{in} + r_s^2 q_{out})}{q_{out}} \left(1 - e^{-\frac{q_{out} t}{S \phi b}}\right)} - y^2 & \text{where } x \geq 0 \\ - \sqrt{\frac{(2r_s b q_{in} + r_s^2 q_{out})}{q_{out}} \left(1 - e^{-\frac{q_{out} t}{S \phi b}}\right)} - y^2 & \text{where } x < 0 \end{cases} \quad [3.12]$$

Here x and y provide the coordinates for a point on the edge of the oblong body.

The value a is defined as $2 \frac{L}{w} - 1$, where $\frac{L}{w}$ is the length to width ratio measured

in the field (note: $\frac{L}{w} \geq 1$). The solution for a was found by combining a half circle

upgradient of the source ($x < 0$) and ellipse, downgradient of the source ($x \geq 0$),

and equating the resulting shape to the entire extent of the LNAPL body. The

shape of pool can be viewed in panel c of Figure 3.6. Draco (1987) presents a similar method for delineating the shape of an LNAPL body following a release.

It is suggested by Draco (1987) that the initial expansion of an LNAPL body is

largely circular as the LNAPL mounds and spreads laterally. As time progresses

the influence of the sloping water table becomes greater and stretches the

downgradient edge of the LNAPL body in the direction of groundwater flow. Due

to the uncertainties with the type of LNAPL and extent of the release, this model

provides a general approximation on the shape and expansion from a continuous source.

At large times equation [3.12] reduces to:

$$x = \begin{cases} a \sqrt{\frac{(2r_s b q_{in} + r_s^2 q_{out})}{q_{out}} - y^2} & \text{where } x \geq 0 \\ - \sqrt{\frac{(2r_s b q_{in} + r_s^2 q_{out})}{q_{out}} - y^2} & \text{where } x < 0 \end{cases} \quad [3.13]$$

Similar to the circular case equations [3.12] and [3.13] are best utilized for point or oblong sources.

From the one-dimensional cross-section, circular, and oblong models it can be seen that with the presence of losses, a constant LNAPL release to the subsurface would result in a finite LNAPL footprint. If the source is found and stopped and the loss rate remains constant, the LNAPL body would begin to shrink.

3.4.2 Fluxes

One-Dimensional – Solutions for LNAPL flux as a function of position are developed by conducting a mass balance using a differential representative elemental volume (REV; Figure 3.7) as shown in the following equation:

$$\frac{dM_{REV}}{dt} = q_{LNAPL_{in}} \rho A_{C_{in}} - q_{LNAPL_{out}} \rho A_{C_{out}} - q_{loss} \rho A_s \quad [3.14]$$

where M_{REV} is the mass (M) of continuous LNAPL in the REV, t is time (T),

$q_{LNAPL_{in}}$ is the upgradient volumetric flux of continuous LNAPL (L/T) entering the

REV, $q_{LNAPL_{out}}$ is the downgradient volumetric flux of continuous LNAPL (L/T)

leaving the REV, q_{loss} is the vertical volumetric flux of LNAPL out of the REV due to losses such as dissolution and evaporation (L/T), $A_{\text{c}_{\text{in}}}$ and $A_{\text{c}_{\text{out}}}$ are the cross-sectional areas (L^2) normal to LNAPL flow into and out of the REV, respectively, and A_s is the surface area (L^2) of the REV exposed to losses. The one-dimensional cross-section REV can be viewed in panel a of Figure 3.7.

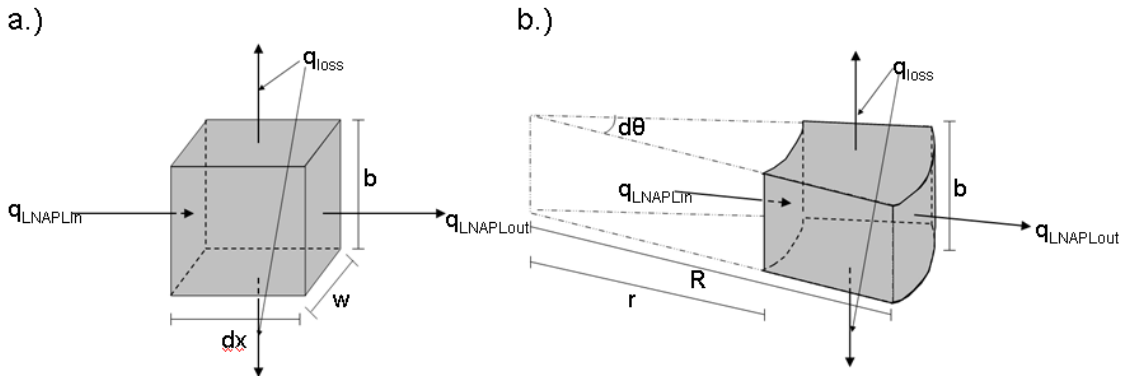


Figure 3.7 - Visual representation of the REVs for the a.) one-dimensional and b.) radially symmetric two-dimensional cases. The one-dimensional case is shown in a.), where Δx is the length, w is the width. The circular and oblong REV is shown in b.), where r is the inner radius of the REV, R is the outer radius of the REV, and θ is the angle of the REV.

For the one-dimensional case the cross-sectional and surface areas are defined in [3.15] and [3.16].

$$A'_{\text{c}_{\text{in}}} = A'_{\text{c}_{\text{out}}} = b \quad [3.15]$$

$$A'_s = dx \quad [3.16]$$

where Δx is the length of the REV (L).

To determine the flux profiles $\frac{dM_{\text{REV}}}{dt}$ is taken to equal zero once the REV is completely filled with continuous LNAPL. This requires the assumption that b , S , and ϕ are constants. With this, once LNAPL completely fills the REV the

LNAPL moving into and out of the REV are equal. The variable q_{LNAPLout} is solved using these assumptions and substituting equations [3.15] and [3.16] into [3.14]. The incremental length Δx is then taken to be any given length of the continuous pool, L , at a given time. The solution for the flux versus position for the one-dimensional is given in equation [3.17].

$$q_{\text{LNAPLout}} = q_{\text{LNAPLin}} - \frac{q_{\text{loss}}L}{b} \quad [3.17]$$

Until the LNAPL body reaches steady-state as a whole, the leading edge of the pool possesses a non-zero flux value. It also follows that this solution is not valid for any location outside of the continuous LNAPL body.

Circular – The same mass balance method was used to determine the circular flux solution (Figure 3.7b). In this case the areas used in equation [3.14] come from [3.18], [3.19], and [3.20].

$$A_{\text{Cin}} = brd\theta \quad [3.18]$$

$$A_{\text{Cout}} = bRd\theta \quad [3.19]$$

$$A_s = \frac{d\theta}{2} [R^2 - r^2] \quad [3.20]$$

where r and R are the radii (L) at which continuous LNAPL enters and exits the REV, respectively, and $\Delta\theta$ is the incremental angle from the centerline.

The flux for a circular body is as follows:

$$q_{\text{LNAPLout}} = \frac{rq_{\text{LNAPLin}}}{R} - \frac{q_{\text{loss}}(R^2 - r^2)}{2bR} \quad [3.21]$$

Oblong – Following the same method as before, equation [3.21] is converted to Cartesian coordinates using the value of **a** (discussed previously). This solution can be found in equation [3.22].

$$q_{\text{LNAPLout}} = \begin{cases} \frac{rq_{\text{LNAPLin}}}{\sqrt{\left(\frac{x}{a}\right)^2 + y^2}} - \frac{q_{\text{loss}}\left(\left(\frac{x}{a}\right)^2 + y^2 - r^2\right)}{2b\sqrt{\left(\frac{x}{a}\right)^2 + y^2}} & \text{where } x \geq 0 \\ \frac{rq_{\text{LNAPLin}}}{\sqrt{x^2 + y^2}} - \frac{q_{\text{loss}}(x^2 + y^2 - r^2)}{2b\sqrt{x^2 + y^2}} & \text{where } x < 0 \end{cases} \quad [3.22]$$

3.4.3 Comparison with Laboratory Data

The one-dimensional length versus time model was compared with the laboratory data to estimate the accuracy of these models (Figure 3.8). The observed steady-state MTBE lengths of the injection rates of 15, 40, 120, and 200 mL/day, with the injection occurring above the water table, were plotted against the predicted steady-state lengths. The discrepancies between the observed and predicted lengths were likely due to slug injections and the small vadose zone in the laboratory experiment. These variations show that a more rigorous verification of the models is needed. Although, these differences are present, the observed lengths follow the trend of the predicted values.

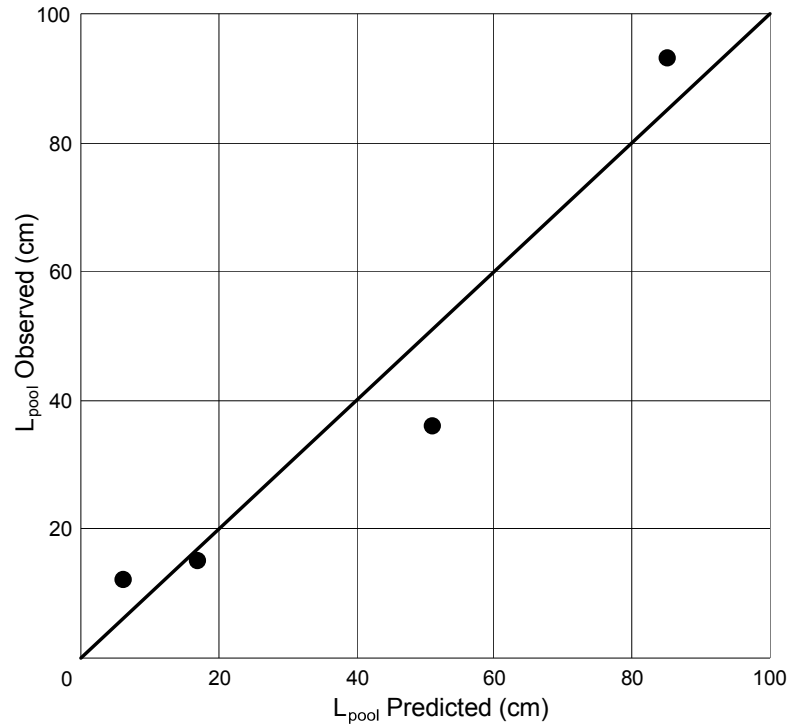


Figure 3.8 - Comparison between the observed steady-state LNAPL lengths and predicted LNAPL lengths.

The authors recognize that these models have limitations due to fluctuations in groundwater depths and thickness of LNAPL bodies over time and space. The models also assumes the LNAPL body is located in homogenous media and has a uniform composition, which in most physical settings is not the case. Another assumption with substantial implications is that of a steady inflow and loss rate of LNAPL. Although, these limitations do exist, these models give a general approximation of the effects of losses to LNAPL bodies in the subsurface.

3.5 Model Application

The following develops a further understanding of the models derived in the previous section. The two critical variables affecting the extent and time frames of these bodies are the LNAPL inflow and loss rates. Mathcad™ 14.0 was utilized for all calculations and Surfer® 9.8 graphing program was used for visualization. In all evaluations LNAPL thickness, source radius, LNAPL saturation, residual saturation of LNAPL, and the porosity of the porous media were constants (0.3 m, 0.3 m, 0.3, 0.001, and 0.3 respectively).

3.5.1 *Extent vs. Time*

The purpose of this analysis was to evaluate influences of natural losses on the expanding and steady-state extent of LNAPL bodies with a constant LNAPL sources. LNAPL loss rates of 5, 10, and 20 m³/ha/yr are considered. These values cover the range of natural rates of LNAPL losses reported by Lundegard and Johnson (2006). Fluxes into the system range from 0.25 to 1 m/yr. The analysis is developed using the scenario of oblong flow. Figure 3.9 presents estimates of LNAPL pool length (L) versus time (panels a, b, and c) and rates of change of the distance from the source to the downgradient edge of the oblong body ($\frac{d(L)}{dt}$) as a function of time (panels d, e, and f).

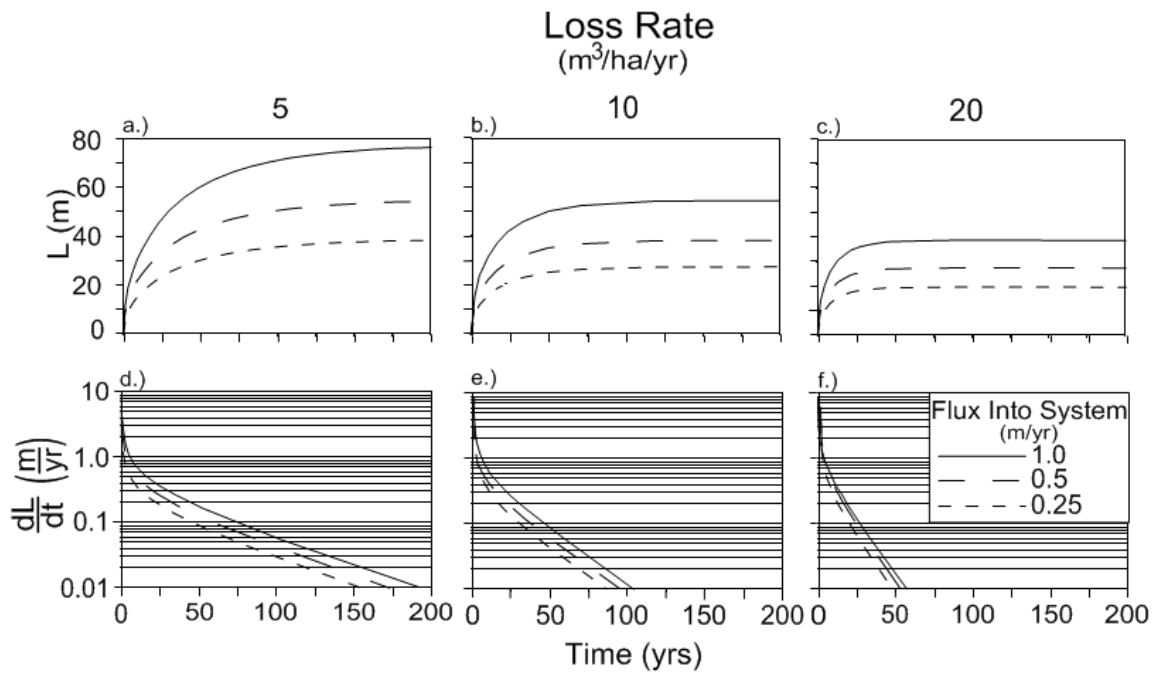


Figure 3.9 - The top panels (a, b, and c) show expansion of the leading edge of the two dimensional oblong body versus time. The bottom panels (d, e, and f) show the change in length per time versus time of the leading edge. Input parameters: $b = 0.3 \text{ m}$, $r_s = 0.3 \text{ m}$, $S = 0.3$, $S_r = 0.001$, $\phi = 0.001$.

It can be seen from the oblong solution that initially the continuous LNAPL body expands quickly and then slows (Figure 3.9 a, b, and c and Figure 3.10). This follows the observed data from the proof-of-concept experiment. The one dimensional and circular models follow this trend as well.

At large times these solutions provide the approximate extent of a stable LNAPL body. A stable LNAPL body was assumed to be reached when the rate of expansion slowed to less than 0.01 m/yr. This assumption was made due to the extremely small change in the extent of the body over time and difficulties with characterizing the inflow rate and area. The panels d, e, and f of Figure 3.9 show the rate of change in length of the leading edge over time. This follows a

similar progression as the proof-of-concept experiment, presented previously.

The time for the LNAPL bodies to stabilize are presented in Table 3.5.

Table 3.5 - Time, in years for a contiguous LNAPL body to stabilize.

		Flux Into System (m/yr)		
		0.25	0.5	1
Loss Rate (m ³ /ha/yr)	5	156.33	174.45	192.70
	10	87.22	96.35	105.53
	20	48.20	52.77	57.37

Figure 3.10 shows as the flux into the system decreases, the time to reach a stable body is slightly less for each loss rate. It can also be viewed that as the loss rate increases the time for the LNAPL body to stabilize is decreased relatively dramatically, when compared to a proportional decrease in the inflow rate. Figure 3.9, Figure 3.10, and Table 3.5 show that the loss rate plays a greater role on time for an LNAPL body become stable, than the LNAPL inflow rate. Thus, by increasing the loss rate to an LNAPL body, the body will reach a stable or shrinking state faster than if the source is lessened by a proportional amount.

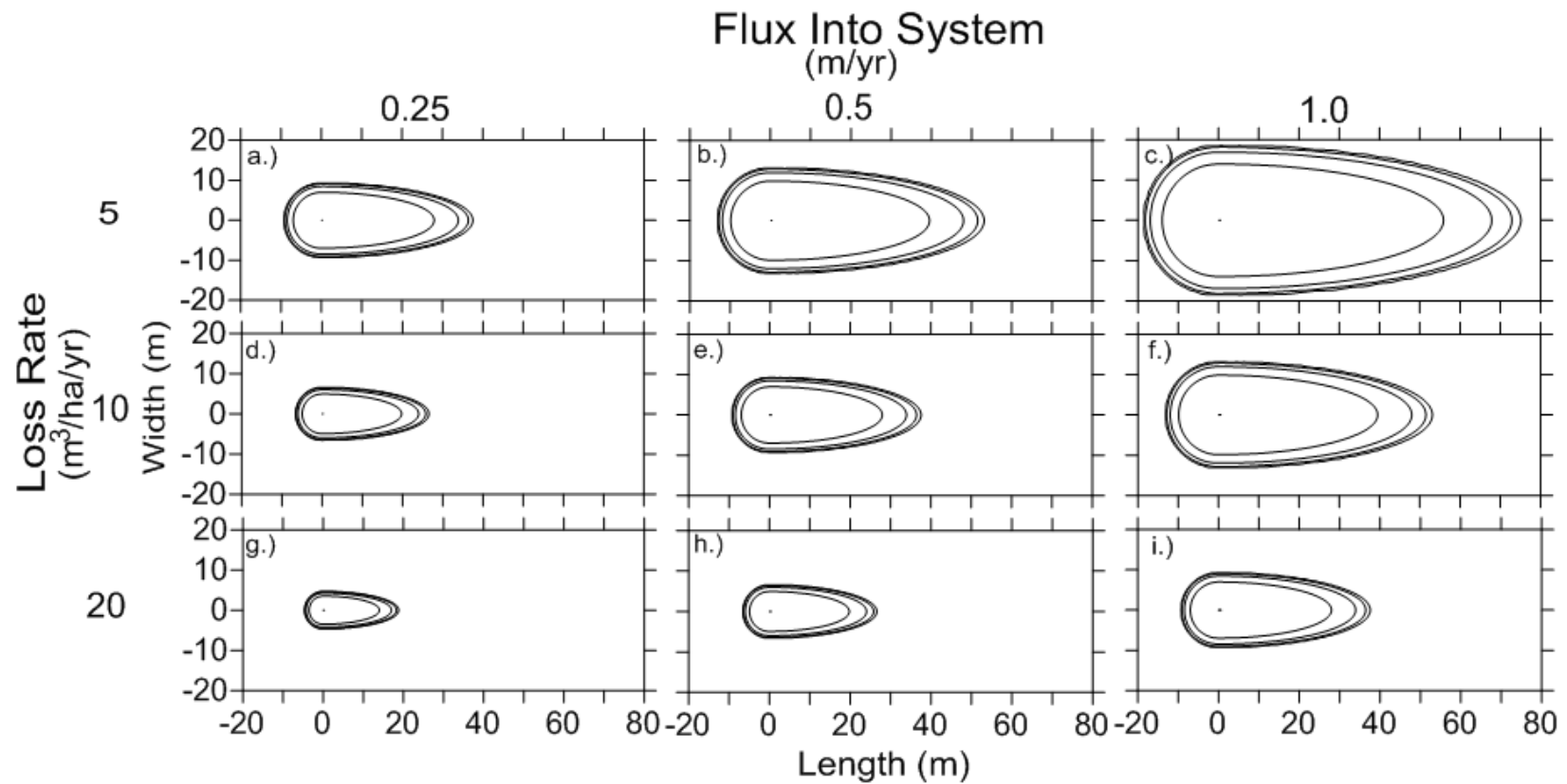


Figure 3.10 - Comparison of the effects of inflow rate and loss rates on the extent over time of an oblong LNAPL body. Input parameters: $b = 0.3$ m, $r_s = 0.3$ m, $S = 0.3$, $S_r = 0.001$, $\phi = 0.001$. The contours are given in years. The contour time increments are: 40 yrs for panels a, b, and c, 20 yrs for panels d, e, f, and 10 yrs for panels g, h, i.

3.5.2 Flux Throughout the LNAPL Body

Flux distributions throughout the extent of the LNAPL body were also investigated. The flux profile of the oblong solution, taken from the center line of the body parallel to groundwater flow, is given in Figure 3.11. This profile shows that the fluxes decrease dramatically and then slow to zero when moving from the source to the edge of the body. Figure 3.12 shows a plan view of the fluxes throughout a continuous oblong LNAPL body. The LNAPL inflow rate was varied from 0.25 to 1 m/yr and the loss rates ranged from 5 to 20 m³/ha/yr. The contours are given in increments of 0.05 m/yr, with the lightest contour representing the flux of 0.01 m/yr. In all cases the LNAPL flux is greatest at the origin (or source location) and decreases to zero at the edge of the pool. As seen in Figure 3.12 the panels diagonal from the upper left to the bottom right of the matrix (a, e, and i) have similar stable extents. Although these similar extents are observed, higher fluxes are observed within the LNAPL bodies that possess larger inflow rates, and vice versa.

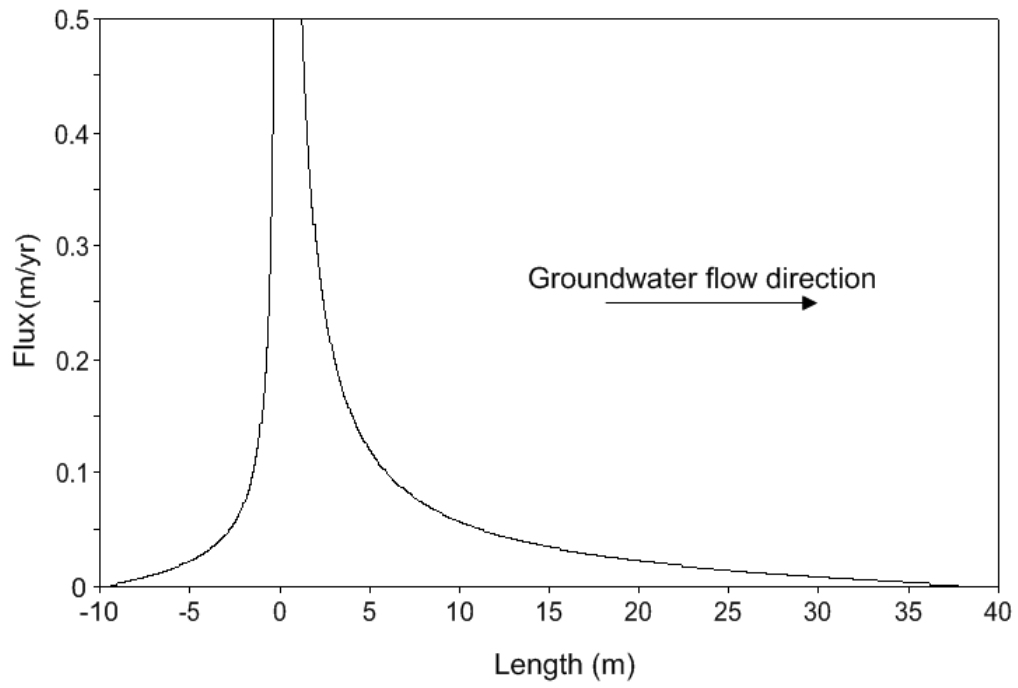


Figure 3.11 - Predicted flux profile of the oblong solution on the center line parallel to groundwater flow.

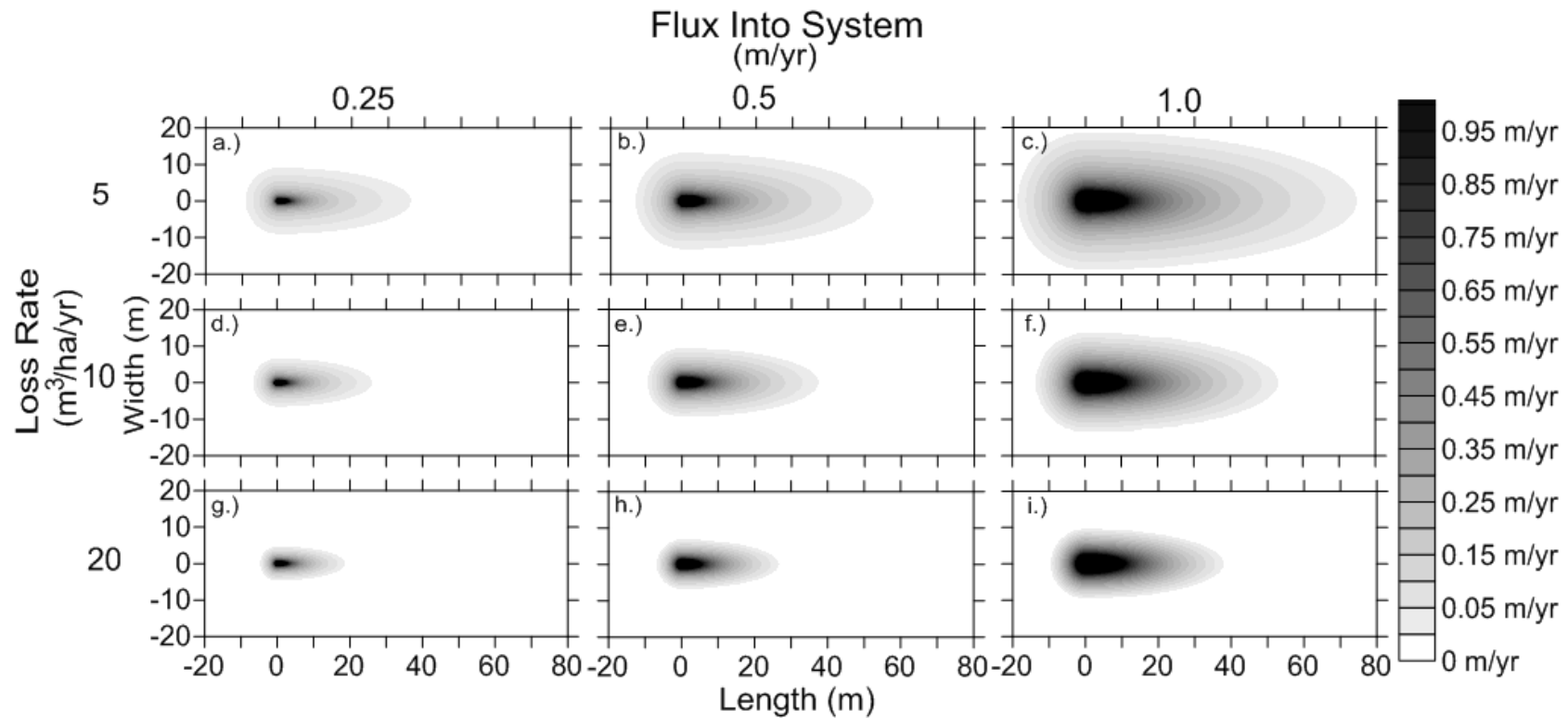


Figure 3.12 - Predicted flux contours over the extent of an oblong LNAPL body, by varying the release rate and loss rate. Input parameters: $b = 0.3 \text{ m}$, $r_s = 0.3 \text{ m}$, $S = 0.3$, $S_r = 0.001$, $\phi = 0.001$.

3.6 Conclusions

Following ITRC (2009) a common regulatory expectation for LNAPL bodies has been LNAPL recovery to the extent practicable. Translating this expectation to quantifiable endpoints can be difficult. Minimum LNAPL thickness in wells has commonly been used as a metric for this. Unfortunately, the relationship between the thickness of LNAPL in a well and the stability of LNAPL in the formation is complex and can be misleading (Sale, 2003). While it has long been recognized that evaporation and dissolution can impact the stability of soil gas and groundwater plumes, the fact losses can also affect the stability of LNAPL bodies as a whole has not been widely recognized.

This paper provides evidence, through a proof-of-concept laboratory experiment and analytical models, that the effects of losses to a continuous LNAPL body can be consequential in the stabilization of the body. From a two-dimensional sand tank experiment it was shown that losses can cause an LNAPL body to stabilize even in the presence of a constant LNAPL inflow. The results from the laboratory experiment suggest natural losses due to evaporation are much greater than that due to dissolution for LNAPL bodies. The analytical models were developed to aid in the explanation of this phenomenon. These models were advanced utilizing a mass balance approach on three geometries: one-dimensional, circular, and oblong. The solutions to the models demonstrated that with a constant inflow these bodies, under the influence of losses, can stabilize. From the flux solutions it was shown that a large portion of the LNAPL body possesses small non-zero flux values of tenths to hundredths of

meters per year. These values are three to five orders of magnitude smaller than groundwater fluxes. With fluxes internal to stable LNAPL bodies it appears the current practice of extrapolating the flux measurements internal to the LNAPL body to the edge of the pool can have significant limitations. The manipulation of the loss rate in these models appears to have more influence on the time required for LNAPL bodies to stabilize, than altering the inflow rate. An alternative method, using these models, may allow for a more reasonable endpoint to the remediation of stable or shrinking LNAPL bodies.

It is worth noting that in the development of the models the assumptions that the media is homogeneous, LNAPL inflow and loss rates do not change over time, and that the thickness of the LNAPL body remains constant are highly idealized. Along with understanding these assumptions, the biggest difficulty in using these models would be determining the rates of natural losses to the LNAPL body. Field conditions are far more complicated. Future work is needed to evaluate the applicability of these models. Once the models have been rigorously verified in the laboratory they should be compared with non-ideal field situations to further test their validity. Also a good method for determining the natural loss rates needs to be devised to utilize the models. A possibility for estimating natural loss rates to a LNAPL body could be by employing the use of solubility or partial pressure data on the LNAPL.

3.7 Acknowledgements

Funding and support for this research was provided by Chevron, Suncor Energy, Exxon Mobil, and the American Petroleum Institute.

4 Conclusions

Petroleum liquids, in the form of fuels, lubricants, and chemical feed stock, have brought great convenience to our modern lives. An unfortunate consequence of our use of petroleum liquids has been inadvertent releases into the subsurface setting. In the subsurface petroleum liquids are referred to as light non-aqueous phase liquids (LNAPLs). LNAPLs have the potential to impact soil gas, groundwater, and surface waters. A drive to remediate and remove continuous LNAPL bodies from the subsurface has resulted. A clear endpoint to remediation of LNAPL bodies has been difficult to ascertain. Obtaining minimum LNAPL thicknesses in wells has commonly been adopted as an endpoint (e.g. ITRC, 2009). The relationship between LNAPL thicknesses in wells to the stability of the continuous LNAPL body is complex (e.g. Farr et al., 1990 and Lenhard and Parker, 1990). This has led researchers to investigate other methods of determining LNAPL stability. LNAPL flux is an attractive metric for evaluating the stability of LNAPL bodies. Two methods to determine LNAPL fluxes have been developed. These include Darcy and single well tracer dilution approaches. The interpretation of measured flux values has been difficult. Fluxes are measured within LNAPL bodies and extrapolated to the leading edge of the bodies. Therefore, if a non-zero LNAPL flux is measured the body is assumed to be migrating at that rate. Conversely, natural losses downgradient

could potentially balance fluxes measured upgradient, and a stable LNAPL body could be present. This thesis explores the possibility of natural losses on the stability of LNAPL bodies.

The first section of this thesis discussed seven field sites where 50 LNAPL fluxes were measured using single well tracer dilution techniques. The magnitudes of the measured LNAPL fluxes and their relationships to LNAPL thickness in wells, LNAPL specific gravity, and distance to the downgradient edge of the LNAPL body were evaluated. Secondly, insight into the possible influence of natural losses was presented through a laboratory proof-of-concept experiment and the development and application of analytical models.

The distribution of the measured LNAPL fluxes at the seven sites was found to range from tenths to hundredths of meters per year. The small LNAPL fluxes imply that the LNAPL bodies are largely stable. No clear relationship was observed between fluxes and LNAPL thicknesses in wells. This seems to contradict the common method of using LNAPL thicknesses in wells as an indicator of the stability of continuous LNAPL bodies. The comparisons between LNAPL flux to the length to the downgradient edge of the body and LNAPL specific gravities also showed no relationship. Although no relationship was observed between LNAPL fluxes and specific gravities of LNAPLs it is likely weathering of LNAPL bodies affects their stability. Assuming these bodies were stable, a one dimensional LNAPL stability model was applied to estimate the losses on these bodies. The majority of the calculated LNAPL loss rates fall above or within the range proposed by Lundegard and Johnson (2006).

It was observed from the proof-of-concept laboratory experiment that with a constant source an LNAPL body can stabilize when the body is exposed to losses due to evaporation and dissolution. This led to the development of analytical models. Three geometries were considered: one-dimensional, circular, and oblong. Models involving the extent of continuous LNAPL versus time as well as fluxes within an LNAPL body were advanced. The models aid in the understanding of the influences of natural loss rates, LNAPL inflow rates, LNAPL thickness, density, saturation, and the porosity of the media. It appears that increasing loss rates decreases the time for an LNAPL body to stabilize greater than a proportional reduction in LNAPL inflow rates. It was seen from these models that fluxes can exist within LNAPL bodies with no lateral expansion or translation. LNAPL fluxes were shown to decrease dramatically moving from the source location to the edges of the LNAPL body.

Although limitations exist and further work is needed with the LNAPL stability models and LNAPL flux measurements, this thesis advances the conceptual idea that natural losses can influence the stability of LNAPL bodies. The combination between small measured fluxes and the potential influence of natural losses on the stability of continuous LNAPL bodies can provide a new performance metric of stable or shrinking LNAPL bodies. The metric of stable or shrinking LNAPL bodies may provide a more pragmatic endpoint in the management of these bodies. However, future work is still needed before this

metric can be fully utilized. Suggestions for future work are discussed in the following section.

5 Future Work

The application of the measured fluxes and the influence of natural losses provides insight into the stability of LNAPL bodies. A pragmatic metric for management of LNAPL bodies could be a stable or shrinking LNAPL body. This section discusses future efforts that are needed for better interpretations of LNAPL flux measurements and development of more rigorous models that address the effects of natural LNAPL losses on the stability of continuous LNAPL bodies.

5.1 Tracer Dilution Flux Measurements

Using tracers to measure LNAPL fluxes have assumptions that limit their use. A constant thickness of LNAPL throughout the duration of the test is desirable to accurately estimate LNAPL flux. Sufficient time between measurements is needed when employing the intermittent mixing technique. The required amount of time needed between measurements lends to a greater possibility in seasonal changes in groundwater elevations. This can result in changes in thicknesses of the LNAPL body.

In tidal zones it is likely that the amount and rates of changes in groundwater elevations cause an averaging of the measured data. Therefore, in

locations with tidal influences the temporally averaged groundwater levels should remain constant. For seasonal settings, LNAPL flux measurements should be taken over the time period of the year when seasonal changes in groundwater levels are at a minimum (autumn and winter). However, measurements only over a portion of a year could skew the results of a single well tracer dilution test. Tracer dilution tests would provide the most accurate understandings of fluxes if the studies were extended over long periods of time. In order to conduct single well tracer dilution tests over extended time periods a better understanding of changes in water table levels on tracer concentrations in LNAPLs would be needed. This could be performed through rigorous laboratory sand tank experiments that evaluate the mechanisms for tracer loss under changing water table conditions.

A combination of a continuously mixed well and intermittent measurements would avoid the difficulties with using the intermittent mixing and measurement procedure. Continuous mixing over the test would prevent short-circuiting of LNAPL within the well and eliminate the need to make measurements before ten percent of the tracer has been lost. Conducting intermittent measurements would reduce man hours and energy needed.

Doubt arose about the detection limit of the instruments used due to the small magnitude of the measured LNAPL flux values. A comprehensive study on the precision, accuracy, and detection limits of the spectrometer is needed to determine an accurate confidence level of the small LNAPL flux measurements.

5.2 Analytical Models

The LNAPL stability models are predicated on a number of limiting assumptions. The models assume LNAPL bodies are located in homogeneous media. Homogeneous media is often only observed in controlled laboratory experiments. It would be expected that a heterogeneous soil would greatly influence the distributions and magnitudes of internal LNAPL fluxes by creating preferential flow paths. Heterogeneous soils would also affect the assumed constant and uniform loss rate throughout the body. The two dimensional models also assume any source feeding the LNAPL body is know and constant. It is often difficult to locate and characterize LNAPL sources. The saturation throughout an LNAPL body is also assumed constant. Differences in pressure through an LNAPL body cause saturations of LNAPL in porous media to vary with depth. Another critical assumption is that LNAPL thickness is constant temporally and spatially. Changes in groundwater elevations could greatly influence LNAPL thicknesses and therefore the accuracy of these models. “Smearing” or vertical spreading of LNAPL would also result from fluctuations in groundwater levels. Concentrations of gaseous petroleum hydrocarbons in the soil pores would be elevated over a larger vertical extent as a result of this spreading. This would reduce the gaseous concentration gradient and decrease the evaporative LNAPL loss rate over time. The removal of the assumptions could be advantageous in practical applications of these models.

The rates of natural LNAPL losses are likely spatially and temporally variable. The physical location of an LNAPL body would likely affect the loss

rates. Depth of LNAPL bodies is a controlling factor on the movement of soil gasses to and from the bodies. Soil heterogeneity also affects soil gas pressures and concentration gradients (Amos et al., 2005). Some LNAPLs are also more susceptible to natural losses than others due to their partial pressure and solubility. Evaporation appears to be the primary mechanism driving losses soon after an LNAPL release. Biodegradation subsequently becomes the dominate mechanism over time (Chaplin et al., 2002). This change in the primary loss mechanism could influence the loss rate temporally. The models do not account for temporal variations in the loss term. These omissions in the loss term would require further research as to the processes that influence natural loss rates. Along with the inclusion of site specific parameters, direct measurements could be used to determine temporally and spatially averaged natural LNAPL loss rates. Amos et al. (2005), Johnson et al. (2006), Lundegard and Johnson (2006), and ongoing studies at Colorado State University have directed their efforts towards measuring natural LNAPL loss rates. Yet further work is still needed.

A possible alternative to analytical LNAPL stability models would be the use of reservoir simulators. This would allow for the effects of natural losses to LNAPL bodies in heterogeneous media to be evaluated. However, the acquisition of data required for reservoir simulators incorporating natural LNAPL losses could be difficult and present limitations to their applicability.

6 References

- Abranovic, D., P.C. Johnson, R.J. Charbeneau, and T.J. Hemstreet (2001). A graphical approach for determining dilution-attenuation factors: basic theory and approach for submerged sources. *Ground Water Monitoring and Remediation* 21, no. 1: 115-124.
- Amos, R.T., K.U. Mayer, B.A. Bekins, G.N. Delin, and R.L. Williams (2005). Use of dissolved and vapor-phase gases to investigate methanogenic degradation of petroleum contamination in the subsurface. *Water Resources Research* 41, no. 2: 1-15.
- Anwar, A.H.M.F., T.H. Tien, Y. Inoue, and F. Takagi (2003). Mass Transfer correlation for nonaqueous phase liquid volatilization in porous media. *Environmental Science and Technology* 37, no. 7: 1277-1283.
- Chaplin, B.P., G.N. Delin, R.J. Baker, and M.A. Lahvis (2002). Long-term evolution of biodegradation and volatilization rates in a crude oil-contaminated aquifer. *Bioremediation Journal* 6, no. 3: 237-255.
- Charbeneau, R.J., R.T. Johns, L.W. Lake, M.J. McAdams (1999). *Free-Product Recovery of Petroleum Hydrocarbon Liquids*. Publication 4682. Washington, D.C.: American Petroleum Institute.
- Draco, T.H. (1987). *Immiscible Transport of Hydrocarbons Infiltrating in Unconfined Aquifers*. In Proceedings of the Symposium of Oil Pollution in Freshwater, Edmonton, Alberta, Canada. 161-175.
- Energy Information Administration (2010). "U.S. Field Production of Crude Oil (Thousand Barrels)". 27 May 2010.
<<http://tonto.eia.doe.gov/dnav/pet/hist/LeafHandler.ashx?n=PET&s=MCRFPUS1&f=M>>
- Eweis, J.B., E.M. Labolle, D.A. Benson, and G.E. Fogg (2007). Role of volatilization in changing TBA and MTBE concentrations at MTBE-contaminated sites. *Environmental Science and Technology* 41, no. 19: 6822-6827.

- Farr A.M., R.J. Houghtalen, and D.B. McWhorter (1990). Volume estimation of light nonaqueous phase liquids in porous media. *Ground Water* 28, no. 1: 48-56.
- Freeze, R. A. and J.A. Cherry (1979). *Groundwater*, Engle Cliffs, NJ: Prentice-Hall Publishing Co.
- Harper, B.M., W.H. Stiver, and R.G. Zytner (2003). Nonequilibrium nonaqueous phase liquid mass transfer model for soil vapor extraction systems. *Journal of Environmental Engineering* 129, no. 8: 745-754.
- Held, R.J. and M.A. Celia (2001). Pore-scale modeling and upscaling of nonaqueous phase liquid mass transfer. *Water Resources Research* 37, no. 3: 539-549.
- Huntley, D. (2000). Analytic determination of hydrocarbon transmissivity from bail-down tests. *Ground Water* 38, no. 1: 46-52.
- Iltis, G. (2007). *Evaluation of Three Methods for Estimating Formation Transmissivity to LNAPL*. M.S. thesis, Department of Civil Engineering, Colorado State University, Fort Collins, Colorado.
- ITRC (Interstate Technology & Regulatory Council) (2009). *Evaluating LNAPL Remedial Technologies for Achieving Project Goals*. LNAPL-2. Washington, D.C.: Interstate Technology & Regulatory Council, LNAPLs Team. www.itrcweb.org.
- Johnson, P.D., P.C. Lundegard, L. Zhuang (2006). Source zone natural attenuation at petroleum hydrocarbon spill sites-I: site-specific assessment approach. *Ground Water Monitoring and Remediation* 26, no. 4: 82-92.
- Kim, J. and M.Y. Corapcioglu (2003). Modeling dissolution and volatilization of LNAPL sources on the groundwater table. *Journal of Contaminant Hydrology* 65, no. 1-2: 137-158.
- Lundegard, P.D. and P.C. Johnson (2006). Source zone natural attenuation at petroleum hydrocarbon spill sites-II: application to a former oil field. *Ground Water Monitoring and Remediation* 26, no. 4: 93-106.
- Lenhard, R.J. and J.C. Parker (1990). Estimation of free hydrocarbon volume from fluid levels in monitoring wells. *Ground Water* 28, no. 1: 57-67.
- Mahler, N.T., T. Sale, and M. Lyverse (2010a). A Mass Balance Approach to Resolving LNAPL Stability. *In final draft, To be submitted to the Journal of Ground Water* July 2010.

- Mahler, N.T., T. Sale, M. Lyverse, and T. Smith (2010b). Single Well Tracer Dilution Tests to Evaluate Field LNAPL Fluxes. *In draft, To be submitted to the Journal of Ground Water* July 2010.
- National Research Council Committee on Intrinsic Remediation (2000). *Natural Attenuation for Groundwater Remediation*. Report, National Academy Press, Washington D.C.
- Pasteris, G., D. Werner, K. Kaufmann, and P. Hohener (2002). Vapor phase transport and biodegradation of volatile fuel compounds in the unsaturated zone: a large scale lysimeter experiment. *Environmental Science and Technology* 36, no. 1: 30-39.
- Sale, T. (2001). *Methods for Determining Inputs to Environmental Petroleum Hydrocarbon Mobility and Recovery Models*. Publication 4711. Washington, D.C.: American Petroleum Institute.
- Sale, T. (2003). *Answers to Frequently Asked Questions About Managing Risks at LNAPL Sites*. API Soil and Groundwater Research Bulletin Number 18. Washington, D.C.: American Petroleum Institute.
- Sale, T., T. Smith, and M. Lyverse (2008). *Direct Measurement of Flow in Porous Media Using Single Well Periodic Mixing Tracer Dilution Tests*, Application Pending March 6th 2008.
- Sale, T., G. Taylor, G. Iltis, and M. Lyverse (2007a). Measurement of LNAPL flow using single well tracer dilution techniques. *Journal of Ground Water*, vol. 45, No. 5, pp. 569-578.
- Sale, T., G. Taylor, and M. Lyverse (2007b). *Measurement of Nonaqueous Phase Liquid Flow in Porous Media by Tracer Dilution*, United States Patent 2007/0113676A1.
- Scholz, D.K., J.H. Kucklick, R. Pond, A.H. Walker, A. Bostrom, and P. Fischbeck (1999). *Fate of Spilled Oil in Marine Waters*, (API) Publication 4691, Washington D.C.: American Petroleum Institute.
- Smith, T., T. Sale, and M. Lyverse (2010). Direct measurement of LNAPL flow using single well periodic mixing tracer dilution tests, *In final draft, To be submitted to the Journal of Ground Water* June 2010.
- Smith, Tim (2008). *Direct Measurement of LNAPL Flow Using Single Well Periodic Mixing Reactor Tracer Tests*, Masters Thesis, Colorado State University, Fort Collins, Colorado.

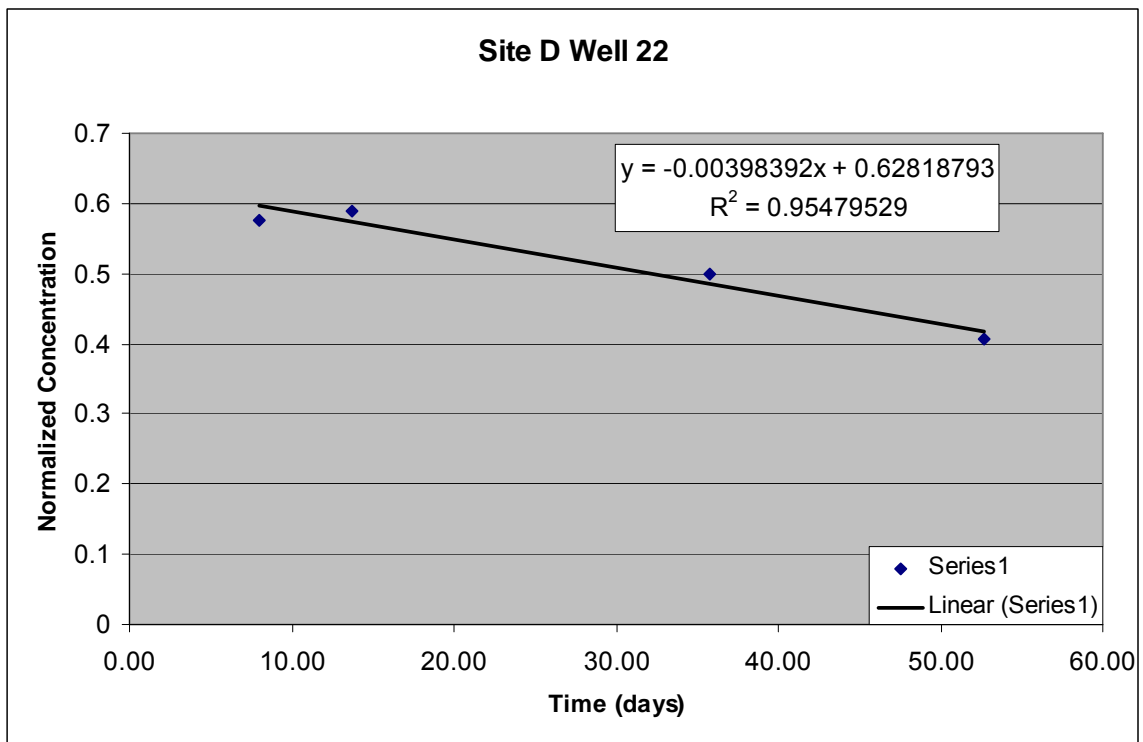
Taylor, G. R. (2004). *Direct Measurement of LNAPL Flow in Porous Media Using Tracer Dilution Techniques*, Masters Thesis, Colorado State University, Fort Collins, Colorado.

Weidemeir, T.H., H.S. Rifai, C.J. Newell, and J.T. Wilson (1999). *Natural Attenuation of Fuels and Chlorinated Solvents in the Subsurface*. Canada: John Wiley and Sons Inc.

Appendix A LNAPL Tracer Dilution Tests

Appendix A.1 Example C_t/C_o Data

Elapsed Time	Depth-to-LNAPL	Depth-to-Water	LNAPL Thickness	C_o	C_{100}	C_{well}	Normalized Concentration
(days)	(m)	(m)	(m)	(intensity)	(intensity)	(intensity)	
8.00	3.21	3.68	0.47	6001	32379	21220	0.58
13.73	3.11	3.60	0.49	5977	32336	21516	0.59
35.78	3.13	3.59	0.46	5197	28172	16683	0.50
52.69	2.99	3.54	0.55	6191	32326	16837	0.41



t_o	t	C_t/C_o		$\frac{q_{LNAPL} * \Delta t}{D}$	q_{LNAPL}	\pm
(day)	(day)	LHS	RHS		(m/yr)	(m/yr)
0.596	1.418	0.701	0.701	0.237	0.098	0.017

Appendix B Laboratory Experiment

Appendix B.1 Proof-of Concept Study Reduced Data

Table B.1 - Reduced proof-of-concept data

		Time (day)	Mass Added (mg)	Dissolved (mg)	Mass Volatilized (mg)	Length (cm)	Mass Loss Rate at SS (mL/day)
9 mL/day	Below WT	0	0.0E+00	0.0E+00	0.0E+00	0	
		1.04	6.7E+03	1.3E-01	6.7E+03	0.94	
		2.06	1.3E+04	2.4E-01	1.3E+04	0.94	
		3.08	2.0E+04	5.9E-01	2.0E+04	0.94	
		5.03	2.7E+04	1.6E+02	2.6E+04	0.94	
		6.06	3.3E+04	2.9E+02	3.3E+04	1.88	
		7.10	4.0E+04	4.4E+02	4.0E+04	1.88	
		8.05	4.7E+04	6.0E+02	4.6E+04	1.88	
		9.06	5.3E+04	7.6E+02	5.3E+04	2.07	
		10.05	6.0E+04	9.2E+02	5.9E+04	2.82	
		11.05	6.7E+04	1.1E+03	6.6E+04	2.82	
		12.08	7.3E+04	1.2E+03	7.2E+04	4.71	
		13.07	8.0E+04	1.3E+03	7.9E+04	4.71	
		14.02	9.1E+04	1.4E+03	9.0E+04	4.71	
15 mL/day	Below WT	15.01	1.0E+05	1.6E+03	1.0E+05	5.18	14.47675
		16.02	1.1E+05	1.8E+03	1.1E+05	5.18	
		17.04	1.2E+05	2.1E+03	1.2E+05	5.65	
		18.06	1.4E+05	2.3E+03	1.3E+05	5.93	
		19.07	1.5E+05	2.6E+03	1.4E+05	6.59	
		20.04	1.6E+05	3.1E+03	1.5E+05	7.06	
		21.01	1.7E+05	3.4E+03	1.7E+05	7.06	
		23.04	1.8E+05	4.2E+03	1.8E+05	7.06	
		24.01	1.9E+05	4.5E+03	1.9E+05	7.06	
		25.09	2.0E+05	4.9E+03	2.0E+05	7.06	
		26.05	2.1E+05	5.3E+03	2.1E+05	7.06	
		27.02	2.2E+05	5.7E+03	2.2E+05	8.00	
		28.03	2.4E+05	6.1E+03	2.3E+05	8.00	
		29.07	2.5E+05	6.5E+03	2.4E+05	8.00	
		30.11	2.6E+05	6.9E+03	2.5E+05	8.00	
		31.04	2.7E+05	7.3E+03	2.6E+05	8.00	
		32.04	2.8E+05	7.7E+03	2.7E+05	8.00	
		33.03	2.9E+05	8.1E+03	2.8E+05	8.00	
		34.03	3.0E+05	8.5E+03	2.9E+05	8.00	
		35.07	3.1E+05	8.8E+03	3.0E+05	8.00	
		36.05	3.2E+05	9.2E+03	3.1E+05	8.00	
		37.02	3.4E+05	9.6E+03	3.3E+05	8.00	
		38.04	3.5E+05	9.9E+03	3.4E+05	8.00	
		39.08	3.6E+05	1.0E+04	3.5E+05	8.47	
		40.08	3.7E+05	1.1E+04	3.6E+05	8.47	

		Time	Mass Added	Dissolved	Mass Volatilized	Length	Mass Loss Rate at SS
		(day)	(mg)	(mg)	(mg)	(cm)	(mL/day)
15 mL/day	Above WT	41.07	3.8E+05	1.1E+04	3.7E+05	8.47	14.780533
		42.07	3.9E+05	1.1E+04	3.8E+05	8.47	
		43.17	4.0E+05	1.2E+04	3.9E+05	8.47	
		44.02	4.1E+05	1.2E+04	4.0E+05	8.94	
		45.07	4.2E+05	1.2E+04	4.1E+05	10.35	
		46.06	4.4E+05	1.2E+04	4.2E+05	10.35	
		47.08	4.5E+05	1.3E+04	4.3E+05	10.35	
		48.07	4.6E+05	1.3E+04	4.4E+05	10.35	
		49.03	4.7E+05	1.3E+04	4.6E+05	10.35	
		50.07	4.8E+05	1.3E+04	4.7E+05	10.35	
		51.08	4.9E+05	1.3E+04	4.8E+05	11.29	
		52.04	5.0E+05	1.3E+04	4.9E+05	11.76	
		53.10	5.1E+05	1.3E+04	5.0E+05	11.86	
		54.13	5.2E+05	1.3E+04	5.1E+05	11.95	
		55.07	5.4E+05	1.4E+04	5.2E+05	11.95	
		56.03	5.5E+05	1.4E+04	5.3E+05	11.95	
		57.01	5.6E+05	1.4E+04	5.4E+05	11.95	
		58.01	5.7E+05	1.4E+04	5.5E+05	11.95	
		59.05	5.8E+05	1.4E+04	5.7E+05	11.95	
		40 mL/day	Above WT	60.04	5.9E+05	1.4E+04	
60.98	6.0E+05			1.4E+04	5.9E+05	11.95	
62.06	6.1E+05			1.4E+04	6.0E+05	11.95	
63.01	6.2E+05			1.5E+04	6.1E+05	11.95	
64.04	6.5E+05			1.5E+04	6.4E+05	11.95	
65.04	6.8E+05			1.5E+04	6.7E+05	11.95	
65.97	7.1E+05			1.5E+04	7.0E+05	11.95	
67.02	7.4E+05			1.5E+04	7.3E+05	11.95	
68.03	7.7E+05			1.5E+04	7.6E+05	11.95	
69.02	8.0E+05			1.5E+04	7.9E+05	12.24	
69.99	8.3E+05			1.6E+04	8.2E+05	12.24	
71.00	8.6E+05			1.6E+04	8.4E+05	12.24	
71.97	8.9E+05			1.6E+04	8.7E+05	12.24	
73.01	9.2E+05			1.6E+04	9.0E+05	12.24	
74.05	9.5E+05			1.6E+04	9.3E+05	14.12	
120 mL/day	Above WT	75.03	9.8E+05	1.7E+04	9.6E+05	14.12	118.72681
		76.03	1.0E+06	1.7E+04	9.9E+05	15.06	
		77.01	1.0E+06	1.7E+04	1.0E+06	15.06	
		78.00	1.1E+06	1.7E+04	1.1E+06	15.06	
		79.02	1.1E+06	1.7E+04	1.1E+06	15.06	
		80.05	1.1E+06	1.8E+04	1.1E+06	15.06	
		81.01	1.2E+06	1.8E+04	1.2E+06	16.00	
		82.01	1.3E+06	1.8E+04	1.3E+06	23.06	
		83.01	1.4E+06	1.9E+04	1.4E+06	23.25	
		84.05	1.5E+06	2.0E+04	1.5E+06	32.00	
		85.77	1.6E+06	2.1E+04	1.5E+06	33.88	
		86.17	1.7E+06	2.2E+04	1.6E+06	34.26	
		87.09	1.7E+06	2.2E+04	1.7E+06	34.82	
		88.09	1.8E+06	2.3E+04	1.8E+06	35.29	
		88.99	1.9E+06	2.4E+04	1.9E+06	35.76	
		90.07	2.0E+06	2.5E+04	2.0E+06	35.95	
		91.01	2.1E+06	2.6E+04	2.1E+06	35.95	
		92.02	2.2E+06	2.7E+04	2.2E+06	35.95	
		92.98	2.3E+06	2.8E+04	2.3E+06	35.95	
		94.10	2.4E+06	2.9E+04	2.3E+06	35.95	
95.04	2.5E+06	3.0E+04	2.4E+06	35.95			
96.01	2.5E+06	3.1E+04	2.5E+06	35.95			
97.07	2.6E+06	3.2E+04	2.6E+06	35.95			
98.00	2.7E+06	3.3E+04	2.7E+06	35.95			
98.96	2.8E+06	3.3E+04	2.8E+06	35.95			

		Time	Mass Added	Dissolved	Mass Volatilized	Length	Mass Loss Rate at SS
		(day)	(mg)	(mg)	(mg)	(cm)	(mL/day)
200 mL/day	Above WT	101.07	3.1E+06	3.6E+04	3.0E+06	35.95	197.46227
		101.98	3.2E+06	3.7E+04	3.2E+06	43.29	
		102.95	3.3E+06	3.8E+04	3.3E+06	53.65	
		104.00	3.5E+06	3.9E+04	3.5E+06	66.82	
		104.94	3.6E+06	4.1E+04	3.6E+06	77.18	
		105.98	3.8E+06	4.3E+04	3.7E+06	77.18	
		107.04	3.9E+06	4.6E+04	3.9E+06	81.88	
		107.96	4.1E+06			83.76	
		109.00	4.2E+06			92.24	
		109.99	4.4E+06			92.24	
		111.00	4.5E+06	5.4E+04	4.5E+06	92.24	
		111.96	4.7E+06	5.5E+04	4.6E+06	92.24	
		113.01	4.8E+06	5.7E+04	4.8E+06	92.24	
		113.93	5.0E+06	5.9E+04	4.9E+06	92.24	
		115.03	5.1E+06	6.1E+04	5.1E+06	92.24	
		115.93	5.3E+06	6.3E+04	5.2E+06	92.24	
		116.86	5.4E+06	6.5E+04	5.4E+06	92.24	
		117.77	5.6E+06			92.24	
118.85	5.7E+06			92.24			
119.94	5.9E+06	7.1E+04	5.8E+06	92.24			

Appendix C Theory

Appendix C.1 One-Dimensional Extent v. Time Derivation

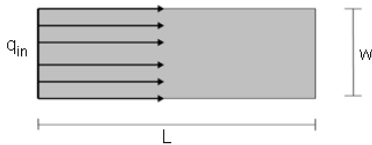
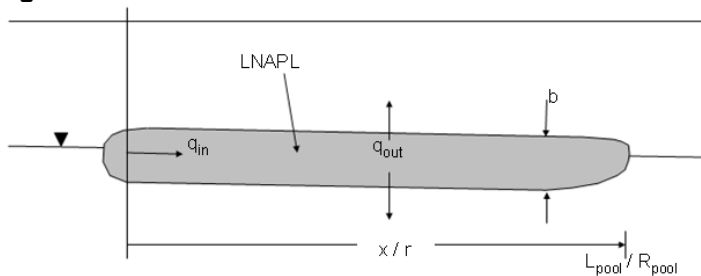


Figure C.1 - One dimensional extent.



Assume one dimensional flow with losses.

To examine the transient-state the pool was examined as a whole. A mass balance performed on the pool as a whole is as follows:

$$M_{\text{Total}} = \int_0^t \text{Inflow} dt - \int_0^t \text{Outflow} dt$$

Where:

$$M_{\text{Total}} = \dot{M}_{\text{Total}} t$$

and

$$\dot{M}_{\text{Total}} = \frac{\rho S \phi b w x}{t}$$

therefore,

$$M_{\text{Total}} = \rho S \phi b w x$$

$$\text{Inflow} = A_c \rho q_{\text{in}} = b w \rho q_{\text{in}}$$

$$\text{Outflow} = A_s \rho q_{\text{out}} = x w \rho q_{\text{out}}$$

Therefore,

$$M_{\text{Total}} = \int_0^t b w \rho q_{\text{in}} dt - \int_0^t x w \rho q_{\text{out}} dt$$

Let M'_{Total} equal mass per unit width, $M'_{\text{Total}} = \frac{M_{\text{Total}}}{w} = \rho S \phi b x$

$$\rho S \phi b x = \int_0^t b \rho q_{\text{in}} dt - \int_0^t x \rho q_{\text{out}} dt$$

Next the derivative is taken of both sides

$$d(\rho S \phi b x) = b \rho q_{\text{in}} dt - x \rho q_{\text{out}} dt$$

Assume that ρ , S , ϕ , b , q_{in} , and q_{out} are all constant

$$\rho S \phi b d(x) = b \rho q_{\text{in}} dt - x \rho q_{\text{out}} dt$$

Separating variables yields:

$$dt = \frac{S \phi b d(x)}{b q_{\text{in}} - x q_{\text{out}}}$$

The integral of both sides is then taken

$$\int_0^t dt = \int_0^{L_{\text{pool}}} \frac{S \phi b}{b q_{\text{in}} - x q_{\text{out}}} d(x)$$

Note: this integral is the same form as $\int \frac{A}{B - Cx} dx$, whose solution is $-\frac{A \ln(B - Cx)}{C}$

Therefore,

$$[t]_0^t = \left[-\frac{S \phi b \ln(b q_{\text{in}} - q_{\text{out}} x)}{q_{\text{out}}} \right]_0^{L_{\text{pool}}}$$

$$t - 0 = -\frac{S \phi b}{q_{\text{out}}} [\ln(b q_{\text{in}} - q_{\text{out}} L_{\text{pool}}) - \ln(b q_{\text{in}} - 0)]$$

$$t = -\frac{S \phi b}{q_{\text{out}}} \left[\ln \left(\frac{b q_{\text{in}} - q_{\text{out}} L_{\text{pool}}}{b q_{\text{in}}} \right) \right]$$

Rearranging and solving for L_{pool}

$$-\frac{S\phi b}{q_{\text{out}}}t = \ln\left(1 - \frac{q_{\text{out}}L_{\text{pool}}}{bq_{\text{in}}}\right)$$

$$e^{-\frac{S\phi b}{q_{\text{out}}}t} = 1 - \frac{q_{\text{out}}L_{\text{pool}}}{bq_{\text{in}}}$$

$$1 - e^{-\frac{S\phi b}{q_{\text{out}}}t} = \frac{q_{\text{out}}L_{\text{pool}}}{bq_{\text{in}}}$$

One-Dimensional Extent v. Time Solution-

$$L_{\text{pool}} = \frac{bq_{\text{in}}}{q_{\text{out}}}\left(1 - e^{-\frac{S\phi b}{q_{\text{out}}}t}\right)$$

Appendix C.2 Two-dimensional extent v. time derivation

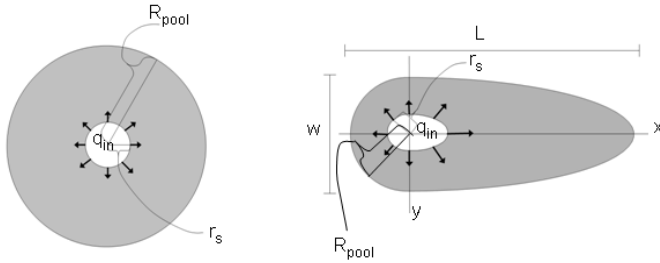
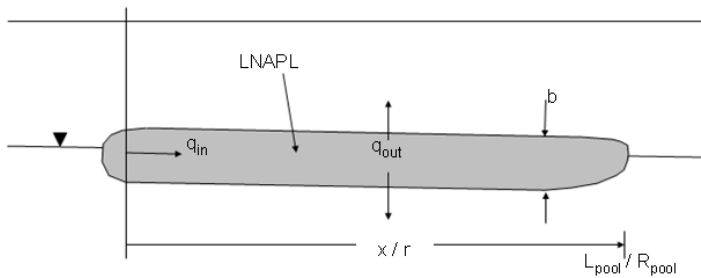


Figure C.2 - Conceptual extent figures for the circular and oblong cases.



Assume two dimensional flow with losses.

To examine the transient-state the pool was examined as a whole. A mass balance performed on the pool as a whole is as follows:

$$M_{\text{Total}} = \int_0^t \text{Inflow} dt - \int_0^t \text{Outflow} dt$$

Where:

$$M_{\text{Total}} = \dot{M}_{\text{Total}} t$$

and

$$\dot{M}_{\text{Total}} = \frac{\rho S \phi b \pi R^2}{t}$$

therefore,

$$M_{\text{Total}} = \rho S \phi b \pi R^2$$

$$\text{Inflow} = A_c \rho q_{\text{in}} = 2\pi r_s b \rho q_{\text{in}}$$

$$\text{Outflow} = A_s \rho q_{\text{out}} = \pi (R^2 - r_s^2) \rho q_{\text{out}}$$

Therefore,

$$M_{\text{Total}} = \int_0^t 2\pi r_s b \rho q_{\text{in}} dt - \int_0^t \pi (R^2 - r_s^2) \rho q_{\text{out}} dt$$

$$\Rightarrow \rho S \phi b \pi R^2 = \int_0^t 2\pi r_s b \rho q_{in} dt - \int_0^t \pi (R^2 - r_s^2) \rho q_{out} dt$$

Next the derivative is taken of both sides

$$d(\rho S \phi b \pi R^2) = 2\pi r_s b \rho q_{in} dt - \pi (R^2 - r_s^2) \rho q_{out} dt$$

Assume that ρ , S , ϕ , b , q_{in} , and q_{out} are all constant

$$\rho S \phi b \pi d(R^2) = 2\pi r_s b \rho q_{in} dt - \pi (R^2 - r_s^2) \rho q_{out} dt$$

Separating variables yields:

$$dt = \frac{\rho S \phi b d(R^2)}{2r_s b \rho q_{in} dt - (R^2 - r_s^2) \rho q_{out} dt}$$

$$dt = \frac{S \phi b d(R^2)}{2r_s b q_{in} + r_s^2 q_{out} - R^2 q_{out}}$$

The integral of both sides is then taken

$$\int_0^t dt = \int_0^{R_{pool}^2} \frac{S \phi b}{2r_s b q_{in} + r_s^2 q_{out} - R^2 q_{out}} d(R^2)$$

$$\text{Let } x_{pool} = R_{pool}^2$$

$$\int_0^t dt = \int_0^{x_{pool}} \frac{S \phi b}{2r_s b q_{in} + r_s^2 q_{out} - x q_{out}} \cdot dx$$

Note: this integral as the same form as $\int \frac{A}{B - Cx} dx$, whose solution is

$$-\frac{A \ln[B - Cx]}{C}$$

Where:

$$A = \rho_{LNAPL} S \phi b$$

$$B = 2r_s b \rho q_{in} + r_s^2 \rho q_{out}$$

$$C = \rho q_{out}$$

Therefore,

$$[t]_0^t = \left[-\frac{A \ln[B - Cx]}{C} \right]_0^{x_{\text{pool}}}$$

$$t - 0 = -\frac{A}{C} [\ln[B - Cx_{\text{pool}}] - \ln[B]]$$

$$t = -\frac{A}{C} \left[\ln \left(1 - \frac{C}{B} x_{\text{pool}} \right) \right]$$

Rearranging and solving for x_{pool}

$$-\frac{Ct}{A} = \ln \left(1 - \frac{C}{B} x_{\text{pool}} \right)$$

$$e^{-\frac{Ct}{A}} = 1 - \frac{C}{B} x_{\text{pool}}$$

$$1 - e^{-\frac{Ct}{A}} = \frac{C}{B} x_{\text{pool}}$$

$$x_{\text{pool}} = \frac{B}{C} \left(1 - e^{-\frac{Ct}{A}} \right)$$

Replacing $x_{\text{pool}} = R_{\text{pool}}^2$

$$R_{\text{pool}}^2 = \frac{B}{C} \left(1 - e^{-\frac{Ct}{A}} \right)$$

$$R_{\text{pool}} = \sqrt{\frac{B}{C} \left(1 - e^{-\frac{Ct}{A}} \right)}$$

Replacing the coefficients A, B, and C yields

Circular Extent v. Time Solution-

$$R_{\text{pool}} = \sqrt{\frac{(2r_s b q_{\text{in}} + r_s^2 q_{\text{out}})}{q_{\text{out}}} \left(1 - e^{-\frac{q_{\text{out}} t}{S \phi b}} \right)}$$

Note:

The pool is stretched by a factor of $\frac{L_{\text{pool}}}{w_{\text{pool}}}$ using the equation for an ellipse:

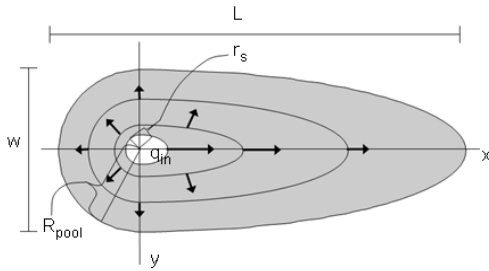
$$1 = \frac{x_{\text{pool}}^2}{(aR_{\text{pool}})^2} + \frac{y_{\text{pool}}^2}{R_{\text{pool}}^2}$$

Where:

$$a = 2 \frac{L_{\text{pool}}}{w_{\text{pool}}} - 1$$

And:

$$L_{\text{pool}} \geq w_{\text{pool}}$$



Solving for the ellipse in Cartesian coordinates yields:

Oblong Extent v. Time Solution-

$$x = \begin{cases} a \sqrt{\frac{(2r_s b q_{\text{in}} + r_s^2 q_{\text{out}})}{q_{\text{out}}} \left(1 - e^{-\frac{q_{\text{out}} t}{S \phi b}}\right)} - y^2 & \text{where } x \geq 0 \\ - \sqrt{\frac{(2r_s b q_{\text{in}} + r_s^2 q_{\text{out}})}{q_{\text{out}}} \left(1 - e^{-\frac{q_{\text{out}} t}{S \phi b}}\right)} - y^2 & \text{where } x < 0 \end{cases}$$

Appendix C.3 One-dimensional flux derivation

a.)

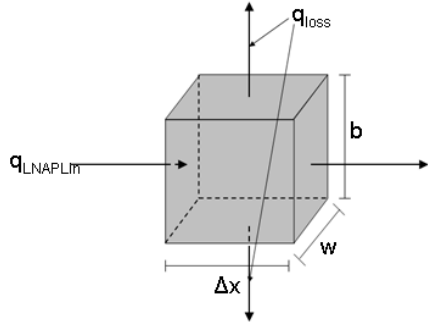


Figure C.3 - REV for one-dimensional flow.

Assume one dimensional flow with losses.

Performing a mass balance length of the pool in question yields:

$$\Delta \text{Storage} = \frac{dM}{dt} = \text{Inflow} - \text{Outflow}$$

Where:

$$\text{Inflow} = A_c \rho q_{\text{LNAPLin}} = bw\rho q_{\text{LNAPLin}}$$

$$\text{Outflow} = A_c \rho q_{\text{LNAPLout}} + A_s \rho q_{\text{loss}} = bw\rho q_{\text{LNAPLout}} + Lw\rho q_{\text{loss}}$$

Thus the equation becomes:

$$\frac{dM}{dt} = bw\rho q_{\text{LNAPLin}} - bw\rho q_{\text{LNAPLout}} - Lw\rho q_{\text{loss}}$$

$$\text{At steady-state } \frac{dM'}{dt} = 0$$

$$0 = bw\rho q_{\text{LNAPLin}} - bw\rho q_{\text{LNAPLout}} - Lw\rho q_{\text{loss}}$$

Rearranging separating variables

$$bw\rho q_{\text{LNAPLin}} = bw\rho q_{\text{LNAPLout}} + Lw\rho q_{\text{loss}}$$

Solving for q_{LNAPLout} yields

One-Dimensional Solution-

$$q_{\text{LNAPLout}} = q_{\text{LNAPLin}} - \frac{q_{\text{loss}}L}{b}$$

Appendix C.4 Two-dimensional flux derivation

b.)

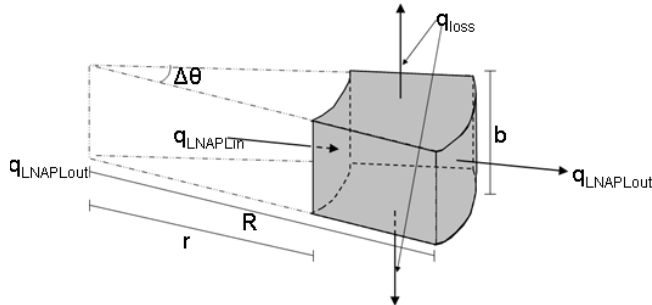


Figure C.4 - REV for two-dimensional flow.

Assume two dimensional flow with losses.

Performing a mass balance on the area of the pool in question yields:

$$\Delta \text{Storage} = \frac{dM}{dt} = \text{Inflow} - \text{Outflow}$$

Where:

$$\text{Inflow} = A_c \rho q_{\text{LNAPLin}} = 2\pi r b \rho q_{\text{LNAPLin}}$$

$$\text{Outflow} = 2\pi R b \rho q_{\text{LNAPLout}} + A_{\text{sl}} \rho q_{\text{loss}} = 2\pi R b \rho q_{\text{LNAPLout}} + \pi(R^2 - r^2) \rho q_{\text{loss}}$$

Thus the equation becomes:

$$\frac{dM}{dt} = 2\pi r b \rho q_{\text{LNAPLin}} - 2\pi R b \rho q_{\text{LNAPLout}} - \pi(R^2 - r^2) \rho q_{\text{loss}}$$

$$\text{At steady-state } \frac{dM'}{dt} = 0$$

$$0 = 2\pi r b \rho q_{\text{LNAPLin}} - 2\pi R b \rho q_{\text{LNAPLout}} - \pi(R^2 - r^2) \rho q_{\text{loss}}$$

Rearranging separating variables

$$2\pi r b \rho q_{\text{LNAPLin}} = 2\pi R b \rho q_{\text{LNAPLout}} - \pi(R^2 - r^2) \rho q_{\text{loss}}$$

Solving for q_{LNAPLout} yields

Circular Flux Solution-

$$q_{\text{LNAPLout}} = \frac{rq_{\text{LNAPLin}}}{R} - \frac{q_{\text{loss}}(R^2 - r^2)}{2Rb}$$

To get the circular flux solution in Cartesian coordinates the equation for the ellipse, seen in the transient two-dimensional oblong extent v. time model was used.

First the equation must be solved for R:

$$q_{\text{LNAPLout}} = \frac{rq_{\text{LNAPLin}}}{R} - \frac{q_{\text{loss}}(R^2 - r^2)}{2bR}$$

$$q_{\text{LNAPLout}}R = rq_{\text{LNAPLin}} - \frac{q_{\text{loss}}}{2b}(R^2 - r^2)$$

$$q_{\text{LNAPLout}}R = rq_{\text{LNAPLin}} - \frac{q_{\text{loss}}}{2b}R^2 + \frac{q_{\text{loss}}}{2b}r^2$$

$$-\frac{q_{\text{loss}}}{2b}R^2 - q_{\text{LNAPLout}}R + \frac{q_{\text{loss}}}{2b}r^2 + rq_{\text{LNAPLin}} = 0$$

$$-\frac{q_{\text{loss}}}{2 \cdot b}R^2 + q_{\text{LNAPLout}}R + \left(\frac{q_{\text{loss}}}{2 \cdot b}r^2 + rq_{\text{LNAPLin}}\right) = 0$$

This is the same form as:

$$aR^2 + bR + c = 0$$

Where:

$$R = \frac{-b \pm \sqrt{b^2 - 4ac}}{2a}$$

Therefore:

$$R = \frac{q_{\text{LNAPLout}} \pm \sqrt{q_{\text{LNAPLout}}^2 + 2 \frac{q_{\text{loss}}}{b} \left(\frac{q_{\text{loss}}}{2b} r^2 + rq_{\text{LNAPLin}} \right)}}{-\frac{q_{\text{loss}}}{b}}$$

$$R = -\frac{q_{\text{LNAPLout}} b}{q_{\text{loss}}} \pm \frac{\sqrt{q_{\text{LNAPLout}}^2 + \left(\frac{q_{\text{loss}} r}{b}\right)^2 + \frac{2q_{\text{loss}} r q_{\text{LNAPLin}}}{b}}}{-\frac{q_{\text{loss}}}{b}}$$

Since R cannot be negative, or smaller than r:

$$R = -\frac{q_{\text{LNAPLout}} b}{q_{\text{loss}}} + \frac{b \sqrt{q_{\text{LNAPLout}}^2 + \left(\frac{q_{\text{loss}} r}{b}\right)^2 + \frac{2q_{\text{loss}} r q_{\text{LNAPLin}}}{b}}}{q_{\text{loss}}}$$

Note:

The pool is stretched by a factor of $\frac{L_{\text{pool}}}{w_{\text{pool}}}$ using the equation for an ellipse:

$$1 = \frac{x_{\text{pool}}^2}{(aR)^2} + \frac{y_{\text{pool}}^2}{R^2}$$

Where:

$$a = 2 \frac{L_{\text{pool}}}{w_{\text{pool}}} - 1$$

And:

$$L_{\text{pool}} \geq w_{\text{pool}}$$

R is converted to Cartesian coordinates using the equation for an ellipse.

$$x = \begin{cases} a \sqrt{\left[-\frac{q_{\text{LNAPLout}} b}{q_{\text{loss}}} + \frac{b \sqrt{q_{\text{LNAPLout}}^2 + \left(\frac{q_{\text{loss}} r}{b}\right)^2 + \frac{2q_{\text{loss}} r q_{\text{LNAPLin}}}{b}}}{q_{\text{loss}}} \right]^2} - y^2 & \text{where } x \geq 0 \\ - \sqrt{\left[-\frac{q_{\text{LNAPLout}} b}{q_{\text{loss}}} + \frac{b \sqrt{q_{\text{LNAPLout}}^2 + \left(\frac{q_{\text{loss}} r}{b}\right)^2 + \frac{2q_{\text{loss}} r q_{\text{LNAPLin}}}{b}}}{q_{\text{loss}}} \right]^2} - y^2 & \text{where } x < 0 \end{cases}$$

Oblong Flux Solution-

$$q_{\text{NAPL}} = \begin{cases} \frac{rq_{\text{LNAPLin}}}{\sqrt{\frac{x_{\text{pool}}^2}{a^2} + y_{\text{pool}}^2}} - \frac{q_{\text{loss}} \left(\frac{x_{\text{pool}}^2}{a^2} + y_{\text{pool}}^2 - r^2 \right)}{2b\sqrt{\frac{x_{\text{pool}}^2}{a^2} + y_{\text{pool}}^2}} & \text{where } x \geq 0 \\ \left[\frac{rq_{\text{LNAPLin}}}{\sqrt{x_{\text{pool}}^2 + y_{\text{pool}}^2}} - \frac{q_{\text{loss}} (x_{\text{pool}}^2 + y_{\text{pool}}^2 - r^2)}{2b\sqrt{x_{\text{pool}}^2 + y_{\text{pool}}^2}} \right] & \text{where } x < 0 \end{cases}$$